The UV-LIDAR: A tool for investigating Aerosol-Cloud Interactions

A case study on Ascension Island

E.V. Tenner

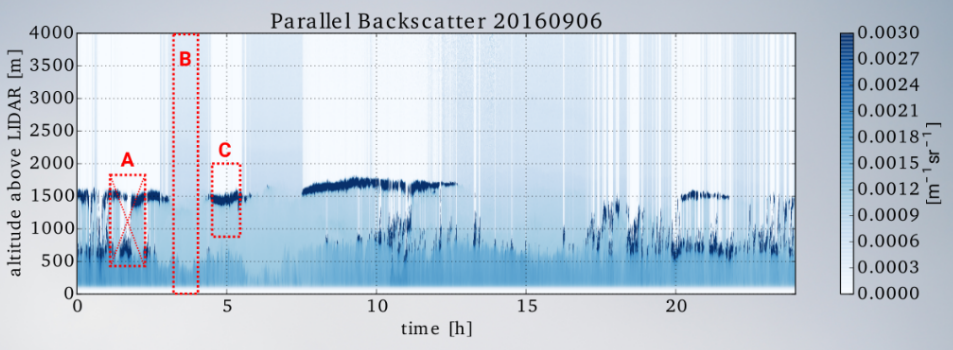

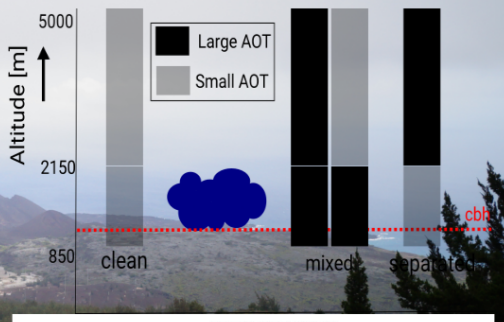

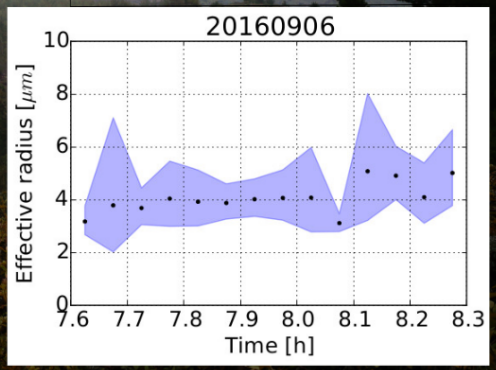

TUDelft

The UV-LIDAR: A tool for investigating Aerosol-Cloud Interactions

A case study on Ascension Island

by

E.V. Tenner

to obtain the degree of Master of Science
at the Delft University of Technology,
to be defended publicly on Friday 7th of July, 2017 at 14:00.

Student number:	4405625	
Thesis committee:	Prof. dr. ir. H.W.J. Russchenberg,	TU Delft
	M. de Graaf,	KNMI
	D.P. Donovan,	KNMI
	ir. C.M.H. Unal,	TU Delft
	A.M.J. Coenders,	TU Delft

An electronic version of this thesis is available at `http://repository.tudelft.nl/`.

TU Delft

Abstract

Climate change and human influences are widely investigated. However, the processes of aerosol-cloud interactions are still not adequately known and the associated lack of knowledge causes uncertainties in climate change prediction. Therefore this study presents different approaches to investigate those interactions, in particular the Twomey-effect, which states that an increase in aerosol loading leads to an increase in cloud drop number density and a decrease in cloud drop effective radius, considering constant liquid water path. The data analysed was obtained during the ASCII campaign 2016 at Ascension Island. Cloud and aerosol measurements were done by an ultra-violet (UV) lidar during the month September 2016. The cloud microphysical properties - cloud drop number density and cloud drop effective radius - were retrieved using the cloud property inversion retrieval algorithm. The cloud effective radius varied between 1.88 and 4.48 μm. The cloud drop number density had values in the range of 228-1690 cm^{-3}. Furthermore, the total aerosol profiles for clear sky scenes and the aerosol profiles below clouds were retrieved, solving the boundary-value-problem using the 'Klett' approach. For the aerosol profiles below clouds an extra factor was introduced, accounting for multiple scattering inside the clouds. The aerosol loading arrived at Ascension Island came mainly from the South (Atlantic Ocean) in the lower 1200m or from the East (African continent, biomass burning events) above 1200m. The aerosol-cloud interactions were examined for both the clear sky and the below cloud aerosols with the cloud properties. Both approaches gave evidence for the Twomey-effect. Those results suggest that the UV-lidar is a suitable instrument for investigation of aerosol-cloud interactions. Future projects can use those approaches to gain more knowledge over the interactions, enabling a major improvement of climate change predictions.

Contents

List of abbreviations

β	Backscatter coefficient
α	Extinction coefficient
R_{eff}	Cloud drop effective radius
ND	Cloud drop number density
IE_r	Indirect Effect parameter for cloud effective radius
IE_N	Indirect Effect parameter for cloud drop number density
AOT	Aerosol optical Thickness
CCN	Cloud Condensation Nuclei
R_{ascat}	Aerosol scattering ratio
S	Extinction-to-backscatter ratio or lidar ratio
$lidar$	Light Detection and Ranging, in this case referred to a UV-lidar instrument
LWP	Liquid Water Path

1 Introduction

During the last decades interest in climate change has increased, resulting in extended research and advanced climate models. Those models incorporate progressively more processes dealing with changes in gases, aerosols and clouds in the atmosphere. Accurately modeling the interaction between aerosols and clouds is a daunting task, because of their short lifetime and heterogeneous distribution [Koch and Del Genio, 2010]. Currently, scientist have poor understanding of these processes. This lack of knowledge is one of the main uncertainties in climate change predictions [Boucher and Zhang, 2013].

The aerosol-cloud interactions can be observed by different instruments and at several places on the globe. There is not one perfect instrument, each technique has its advantages and disadvantages. For example, space-borne measurements are useful, because of their global coverage. Unfortunately, the time resolution varies from once per 15-30 minutes for geostationary satellites, to once per day or a couple of days for polar orbiting satellites. In addition to that the distinction between clouds and aerosols can be challenging from space. Several investigations are executed using satellite data e.g. on shallow cloud development [Kaufman et al.], on cloud properties [Min and Harrison, 1996], on biomass burning aerosol indirect effects on clouds [Brioude et al., 2009] and on aerosol retrieval above clouds [de Graaf et al., 2012],[de Graaf et al., 2014]. Besides that, for small scale processes like the microphysical changes of clouds, small scale measurements are preferred [McComiskey and Feingold, 2012]. Airborne techniques can measure aerosols and clouds in detail using in situ or remote sensing techniques. It should be stressed that such measurements are scarce and bounded by specific campaigns, such as the SAMUM campaigns on Saharan dust and biomass burning aerosol characteristics [Amiridis et al., 2009], [Tesch et al., 2011]. Ground-based measurements can probe the atmosphere very locally. The time resolution can be high, so the fast changes in aerosols and clouds can be detected.

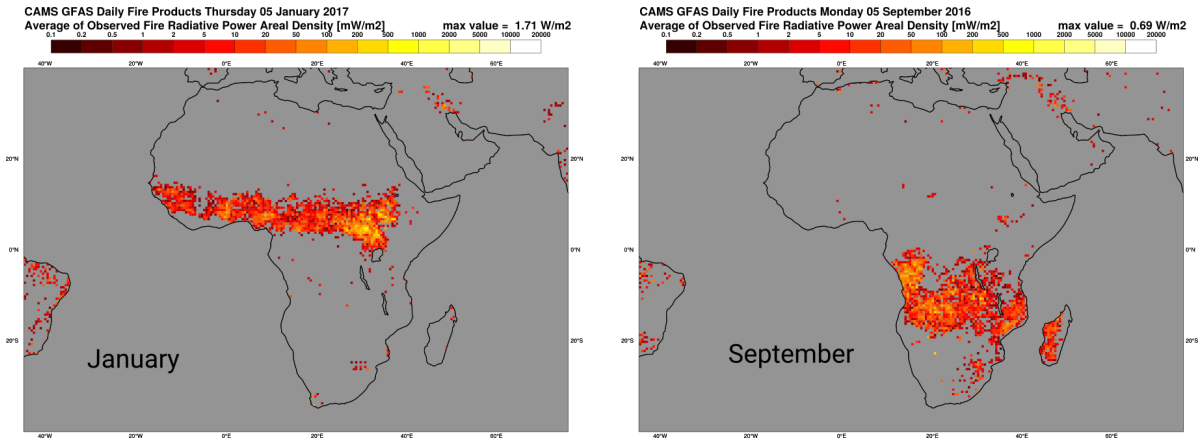

Figure 1.1: The average of observed fire radiative power for 05 January (left) and 05 September (right). The lighter the pixel, the more fires were detected. Source: CAMS GFAS fireproduct.

Lidar (LIght Detection And Ranging) is such an instrument that can be used to study different aspects of clouds and aerosols, for example, dust and smoke transport [Ansmann and Muller, 2005], aerosol optical characteristics [Amiridis et al., 2009] or the extinction-to-backscatter ratio [Müller et al., 2007]. Some of the research performed on the topic of aerosol-cloud interaction used a combination of instruments, like a lidar, radar and radiometer [Sarna and Russchenberg, 2016],[Kim, 2003], [Min and Harrison, 1996]. In the present study, a ground-based UV-lidar is used to obtain cloud properties and aerosol profiles.

For the measurement location an adequate number of aerosols and the presence of clouds are mandatory. A large source of aerosols is biomass burning; in 2000 the global average emission of biomass burning aerosols was 49.1 $Tgyr^{-1}$, whereby Africa had the largest average contribution of $23.9 Tgyr^{-1}$[Boucher and Zhang, 2013]. In Figure 1.1 the seasonal variation of the fire events in Africa is shown. This seasonality followed from the global circulation, whereby the inter tropical convergence zone (ITCZ) shifts from above the equator (July) to below the equator (January), resulting in wet season where the ITCZ is and a dry season otherwise. During summer (September) the dry season is in the south, resulting in the most fires in the south, while during winter (January) the northern part is the driest and burns. The biomass burning events emit black carbon aerosols into the atmosphere, which are absorbing aerosols and these can also function as cloud condensation nuclei [Koch and Del Genio, 2010]. The prevailing wind from Africa is westward, carrying the aerosol load over the South East Atlantic, whereby the aerosol load is the largest during summer [Swap, 1996]. The dominating clouds over this region are shallow clouds marine stratocumulus clouds. They are widespread, which makes them the most favorable cloud type for research into the behavior of clouds [Kim et al., 2003], because these clouds are sensitive to changes in aerosol concentrations [Brioude et al., 2009].

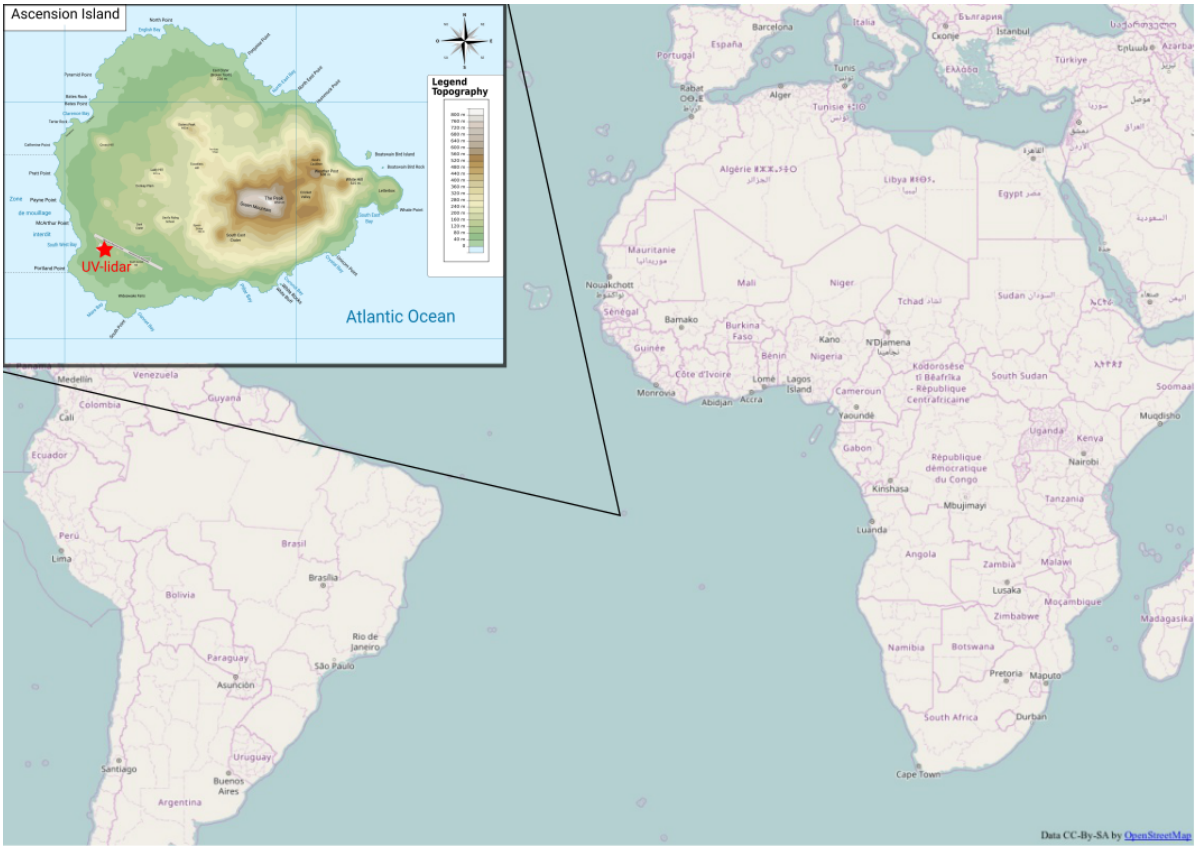

Figure 1.2: Overview of the location of Ascension Island. The red star represents the location of the UV-lidar. Image from wikipedia: https://commons.wikimedia.org/w/index.php?curid=11767299

This study focuses on aerosol-cloud interaction above Ascension Island. This island, located in the Atlantic Ocean (see Figure 1.2), is exceptionally suitable for research on aerosol-cloud interaction, because of the high cloudiness and the varying aerosols coming from biomass burning in Africa [Hegg et al., 2012],[Kaufman et al.],[Swap, 1996]. During the month of September in 2016 the measurement campaign Ascension Island Initiative (ASCII) was organized by the Technical University of Delft and the Royal Netherlands Meteorological Institute (KNMI). During this campaign a ultra-violet (UV) depolarization lidar was deployed on the island to measure the clouds and aerosols in the atmosphere. In the same period other research campaigns in the same area and on the same topic were operated including LASIC (layered Atlantic smoke interactions with clouds) [LASIC] and NASA-ORACLES (observations of aerosols above clouds and their interactions) [ORACLES].
The goal of the ASCII campaign is:

" (..) to obtain new observations on cloud formation processes, over the south-east Atlantic Ocean, which is a unique natural laboratory to study the effect of smoke on clouds. This goal is achieved by 1) deploying a sophisticated lidar instrument on a remote island in the South Atlantic Ocean; 2) implementing and testing a new retrieval technique; 3) sharing of data with campaign project partners and validation of the method." [Sarna et al., 2016]

This masters thesis project is part of the ASCII project and has the following research questions:

1. How can aerosol-cloud interaction be investigated using just one instrument: the UV-lidar?
2. What is the impact of African smoke on cloud formation above Ascension Island?

To investigate aerosol-cloud interactions we needed a description of the cloud and aerosols. In this research the strength of the UV-lidar to retrieve information from both variables (the cloud and the aerosols) was used. The clouds were described by the cloud effective radius, cloud drop number density and cloud base height. We extracted those properties from the lidar measurements using a cloud property inversion retrieval algorithm. The cloud retrieval algorithm exploits the dependence of the multiple-scattering induced depolarization on the cloud properties [Donovan et al., 2015]. The aerosols can be described by their extinction profiles, which can be used to calculate the aerosol optical thickness. In order to obtain those extinction profiles we developed a retrieval algorithm based on the Klett-Fernald theory [Klett, 1984], which is valid for clear skies only. We modified the algorithm so we could also retrieve the aerosol profiles below the clouds. In order to do so, the cloud extinction was needed, which we got from the cloud property inversion retrieval algorithm. From that point we had both cloud properties and a proxy for the aerosol load. We examined three different approaches to study the aerosol-cloud interactions.

This report starts with a short introduction covering aerosols, cloud formation and the instrumentation. Next the cloud property inversion retrieval algorithm is described, followed by the aerosol retrieval algorithm. Then the aerosol proxy and the cloud properties are compared and the aerosol-cloud interactions are explained. Finally, I present the conclusions of this project.

2

Background and instrumentation

2.1. Aerosols

Aerosols are solid and liquid particles in the atmosphere. They can be of almost any size, shape and composition, also varying during their lifetime. Strictly speaking, cloud droplets and precipitation are also aerosols, but we do not view them as such here. Aerosols are widely available in the atmosphere and have different sources, such as combustion, sea spray, volcanic eruption and forest fires. The lifetime of an atmospheric aerosol is typically between a day till about two weeks for aerosols in the troposphere. If aerosols reach the stratosphere, then the typical lifetime increases to about a year [Boucher and Zhang, 2013].

Aerosols can have several effects on the energy balance of the earth. First they have a direct effect on the atmosphere by absorbing and scattering solar radiation. Scattering of the light results in a cooling effect, while absorption is associated with warming of the atmosphere [Boucher and Zhang, 2013]. Furthermore, they can interact with the atmosphere for example as Cloud Condensation Nuclei (hereafter CCN) for cloud formation. A cloud droplet is formed when water condenses around a CCN. The cloud microphysical properties depends on the type of the aerosol. Thus a change in aerosol loading can cause a change in cloud microphysics. This effect is known as the Twomey effect, first indirect effect or albedo effect. Twomey discovered that an increase in aerosols lead to an increase in cloud drop number density. Considering the same liquid water path the size of the droplets will drop [Twomey, 1977a]. Moreover, the higher number of smaller droplets results in an increase in the cloud optical depth. An increase in cloud optical depth means an increase in cloud albedo, because the smaller droplets can reflect more of the solar radiation than larger droplets can. Besides the increase in albedo, the lifetime of a cloud can be changed as well, because this depends on the cloud properties and the removal processes. Precipitation is one way a cloud is removed from the atmosphere. However, precipitation occurs only when the droplets are large enough. Therefore this effect should increase the lifetime of the cloud. If all clouds were similarly influenced by this principle, then it would result in an increase in the average cloud coverage of the earth.

Finally, the interaction of the aerosol with clouds depends on the location of the aerosol loading with respect to the cloud. If the aerosol layer is above the cloud, then the cloud is influenced in a semi-direct fashion. The aerosol layer alters the atmosphere by absorbing and/or scattering radiation, which causes a warming or cooling effect. Depending on the state and altitude of the cloud, the cloud formation is enhanced or suppressed [Koch and Del Genio, 2010], [Kaufman et al.], [Brioude et al., 2009], [Kim et al., 2003].

As can be understood from the overview presented above, the aerosol impact on the atmosphere is a complex system. It depends partly on the aerosol type, the vertical distribution relative to the cloud and the cloud itself [Brioude et al., 2009]. These processes and effects lead to one of the greatest uncertainties of the earths energy budget [Boucher and Zhang, 2013]. In this research we shall focus on the Twomey effect.

2.2. Cloud formation

Clouds are formed by several processes in the atmosphere. Here a basic introduction about the cloud formation is given, a more complete explanation can be found in [Salby, 1995] and [Twomey, 1977b]. Cloud droplets are formed when water vapour condensates in the atmosphere. Aerosols are crucial in this process, because in nature it is not possible for water vapor to form a droplet without a surface to condensate on. Aerosols can act as such surfaces, therefore known as cloud condensation nuclei (CCN). Nevertheless, the meteorological

variables such as amount of water vapour, temperature and pressure are important. Depending on the state of the atmosphere water vapor is able to condensate. An amount of air with a particular temperature can contain a specific amount of water vapor and the laws of Clausius-Clapeyron dictate that warmer air can contain more water vapor than colder air. A decrease in temperature, results in an increase in water vapor pressure which increases the possibility for water vapor to condensate (cloud formation). However, a threshold value of water vapor pressure is needed, before condensation occurs. This threshold value depends primarily on the type and properties of the CCN. The more hygroscopic, soluble or larger the CCN, the lower the threshold value. The number of droplets formed is proportional to the number of CCNs. The size of the droplets depends mainly on the amount of available water vapor. The altitude at which the relative humidity reaches the saturation level and droplets could be formed is called the cloud base height. Droplets are formed first couple of meters in the cloud [Pinsky et al., 2012], higher in the cloud other processes occur. Such processes are droplets growth by condensation or collision, or shrink by evaporation, depending on the amount of water vapor in the air.

There are roughly three classes of clouds. Stratiform clouds are developed by sloping convection, whereby a warmer air mass is lifted due to a collapse with a colder air mass. The temperature of air drops by ascending, so the water vapor pressure increases. Those clouds form layers and are characterized by number densities of 300 cm^{-3} and radii of 4 μm. Cumuliform clouds are also developed by rising air, but the air mass ascends due to the warming of the air at the surface. Those clouds can have large cloud droplets. The last cloud type is called cirriform and is mostly found at high altitudes. Those clouds are characterized by small number density, but large radii (~ 250 μm) while consisting of ice particles. [Salby, 1995]

In general water clouds below 3 km altitude will have drop number densities from 10 cm^{-3} till a couple of thousand per cm^{-3}, whereby a distinction can be made between continental air, with number densities around 200-2000 cm^{-3} and marine air, with number concentrations around 20-200 cm^{-3}. The drop radii in a cloud with a number density of 100 cm^{-3} are between 4.2-13 μm, while the droplets in a cloud with a number density of 1000 cm^{-3} are in a range of 1.9-6 μm. Those values are theoretically and depending on the liquid water content, which ranged between respectively 0.03 g/m^3 and 1 g/m^3 for the above mentioned values of the cloud properties[Twomey, 1977b].

In this study we assume stratiform clouds over marine area but with an influence of continental air, so we expect to observe a cloud drop number density around the 20-2000 cm^{-3} with a radius with minimum of 1.9 μm and a maximum of 13 μm, depending on the liquid water content.

2.3. Instrumentation

2.3.1. UV-LIDAR

The UV-lidar used in the ASCII campaign is a ground-based ALS-450 LIDAR manufactured by LEOSPHERE [LEO, 2007]. The laser was pointed vertically with a zenith angle of 3 degree and has a wavelength of 355 nm. The overlap of the laser beam and the receiver is around 200 m altitude. The temporal resolution is 30 s and the range resolution 15 meters. The maximum altitude measured was 20 km. The UV-lidar was located next to the UK meteorological office on Ascension Island (7°58'10.3"S 14°24'19.8"W) at an altitude of 85 meters above mean sea level. During this campaign 24 days were measured successfully.

Lidar principles

Lidar is an active remote sensing instrument, which transmits a light pulse into the atmosphere and receives the backscattered part of the pulse. The backscatter is detected as a function of time. The distance from which the return signal originated is calculated using:

$$z = \frac{ct}{2}, \tag{2.1}$$

where c is the speed of light and t the time difference between transmitting and receiving. It is divided by 2 to account for the two-way-travel of the pulse. The pulse interacts with the particles in the atmosphere and part of the signal will be scattered back in the direction of the instrument, as illustrated in Figure 2.1A.

The interaction of the pulse with the particles can be absorbing and/or scattering depending on the properties of the particle (e.g. size, shape, composition) and the wavelength. For particles with diameter D smaller than the wavelength λ, e.g. atmospheric molecules, ($\lambda >> D$) Rayleigh scattering occurs, the particle backscatter is proportional to λ^{-4} and the scattering is equally distributed in forward and backward direction. The scattering properties of particles with a size of the same order of magnitude as the wavelength can be described using Mie theory [Raymond, 1984].

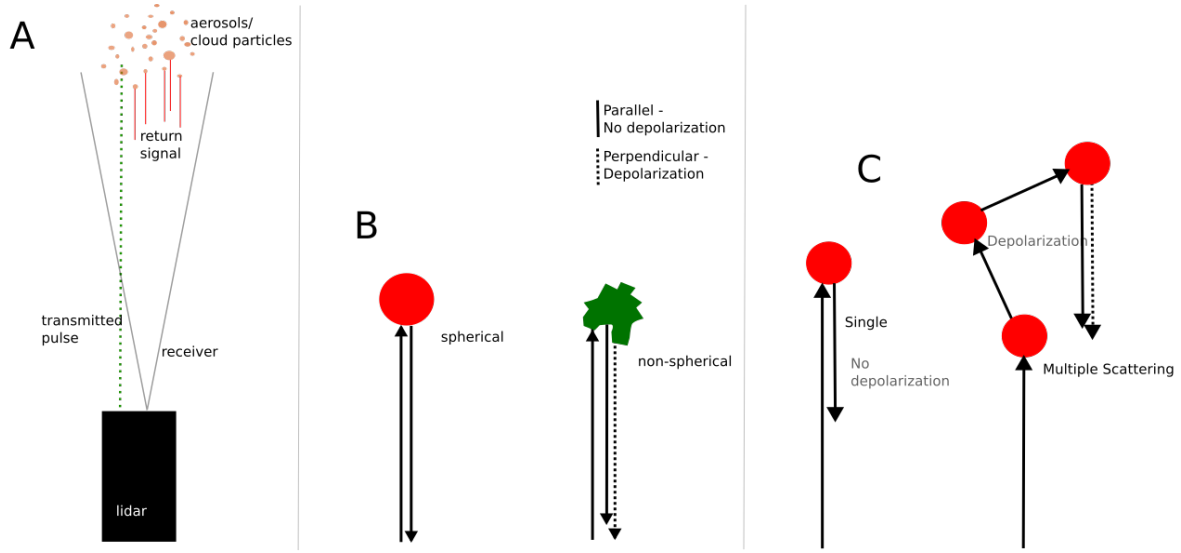

Figure 2.1: Schematic representation of lidar principle and depolarization. A) The instrument transmits a light pulse into the atmosphere, the atmospheric particles, such as aerosols or cloud particles, return part of the signal back towards the lidar. Then the receiver detects and records the return signal. B) The principle of depolarization caused by particle shape. The spherical particle return is non-depolarized, so only contains the parallel signal, while the non-spherical particle depolarizes the signal and returns both polarizations, parallel and perpendicular. C) The left-handside shows single scattering, no depolarization occurs. The right-handside shows multiple scattering. The pulse is scattered by multiple particles before returning to the Lidar, the off axis scattering events results in a depolarized signal event when only spheres are involved.

The total return power is a function of the atmospheric scattering properties:

$$P(z) = \frac{C_{lid}}{z^2}(\beta(z))e^{-2\int_0^z \alpha(z'))dz'}, \tag{2.2}$$

where P is the power received by the instrument, z is the altitude from the instrument in line of sight (Eq.2.1), C_{lid} is the lidar calibration coefficient, β is the atmospheric backscatter coefficient and α is the atmospheric extinction coefficient. The atmospheric backscatter coefficient and atmospheric extinction coefficient can be divided into a molecular, aerosol and cloud part (denoted with the subscripts m, a, c respectively),

$$\beta = \beta_m + \beta_a + \beta_c, \tag{2.3}$$

and

$$\alpha = \alpha_m + \alpha_a + \alpha_c. \tag{2.4}$$

The attenuated backscatter (ATB) is the signal corrected for the range:

$$ATB(z) = z^2 P(z). \tag{2.5}$$

In the case of single-scattering, the backscattered radiation from spherical particles retains its polarization state, while non-spherical particles depolarize the signal, as illustrated in Figure 2.1B. Also multiple scattering leads to depolarization (Figure 2.1C), because the off axis scattered beam from a spherical particle is depolarized, as revealed by the Mie theory, and this beam is through multiple scattering redirected back to the lidar [Pal and Carswell, 1985]. Our lidar instrument distinguishes between parallel and perpendicular polarization when receiving the pulse. A linearly polarized laser beam is transmitted and the return signal is detected by two separated detectors, one for the parallel polarized signal and the other one for the perpendicular part of the signal. The sum of the parallel and the perpendicular return gives the total return. The ratio between the parallel and perpendicular signal is called depolarization ratio.

2.3.2. Balloon-borne sounding system

The balloon-borne sounding system measured, in situ, the vertical profiles of the temperature, pressure and the relative humidity (i.e.thermodynamic state of the atmosphere). Radiosondes were launched 8 times a day by the atmospheric radiation measurement (ARM) climate research facility at Ascension Island. We needed

these variables for each altitude and time measurement of the lidar. Therefore, the radiosonde measurements were interpolated in time and altitude. The interpolation of the pressure with height was done logaritmically, while the interpolation of pressure with time was linearly interpolated. The temperature was linearly interpolated with height and time.

Furthermore, the molecular extinction and backscatter coefficients were calculated. The molecular backscatter coefficient was calculated by

$$\beta_m = \frac{\rho_{atm}}{M}\left(\frac{\lambda}{550}\right)^{-4.09} 10^{-32}, \tag{2.6}$$

where λ is the wavelength in nm, which is in our case 355nm and M the average molecular mass of air ($4.81e-26kg$) and β_m got the units $m^{-1}sr^{-1}$ [Collis and Russell, 1976]. The atmospheric density (ρ_{atm}) was obtained by

$$\rho_{atm} = \frac{p}{T}\frac{1}{\rho_{dryair}}, \tag{2.7}$$

where p is the measured pressure in Pa, T the measured temperature in K and ρ_{dryair} is the gas density of dry air with a value of 287 $J/kg/K$. From the molecular backscatter coefficient the molecular extinction coefficient is calculated as in Eq. 2.13, with the extinction-to-backscatter ratio of $\frac{8\pi}{3}$sr [Raymond, 1984].

2.4. Aerosol and cloud parameters

This section will describe the main parameters used for the description of aerosols and clouds. The aerosol loading can be described by different proxies. In this research we obtained the aerosol extinction coefficient (α), aerosol backscatter coefficient (β), aerosol scattering ratio (R_{ascat}) and aerosol optical thickness (AOT). Proxies e.g. the Cloud Condensation Nuclei (CCN), aerosol size, age and composition are beyond the scope of this study. The aerosol scattering ratio (R_{ascat}) can be calculated from the aerosol backscatter coefficient and the molecular backscatter coefficient:

$$R_{ascat} = \frac{\beta_a + \beta_m}{\beta_m}. \tag{2.8}$$

The aerosol scattering ratio has a value of 1 if there are no aerosols. The Aerosol Optical Thickness (AOT) is a frequently used parameter in research on radiation and can be calculated from the aerosol extinction profile;

$$AOT = dz \sum_{i=z_1}^{z_2} \alpha_i, \tag{2.9}$$

whereby dz is the height of a lidar range bin, α the aerosol extinction, z_1 the lower altitude and z_2 the upper altitude.

In order to describe a cloud commonly used terms are the cloud effective radius, cloud drop number density, cloud extinction and cloud base height. The cloud effective radius (R_{eff}) is defined as:

$$R_{\text{eff}} = \frac{\int n(r) r^3 dr}{\int n(r) r^2 dr}, \tag{2.10}$$

where r is the drop radius and $n(r)$ the drop size distribution. Furthermore there is the Indirect Effect parameter (IE) used to describe the aerosol-cloud interactions [Feingold et al., 2001]. This parameter was formulated by Feingold et al. [2001] to empirically quantify the aerosol indirect effect as described by Twomey [1977a]. This parameter describes the relative change of the cloud properties against the relative change in aerosols. For the cloud effective radius:

$$IE_r = -\frac{d\ln R_{\text{eff}}}{d\ln \alpha}. \tag{2.11}$$

For the cloud drop number density:

$$IE_N = \frac{d\ln ND}{d\ln \alpha}, \tag{2.12}$$

whereby for both cases the α is the aerosol proxy, which can be the aerosol extinction or the aerosol optical thickness or other aerosol equivalent. In our case the AOT was used. Another parameter that is used for all particles (including clouds, aerosols and molecules), is the extinction-to-backscatter ratio or lidar ratio.

$$S = \frac{\alpha}{\beta}. \tag{2.13}$$

This ratio depends on the particle properties, e.g. composition, size and age.

3

Cloud properties

In this chapter a description of the processing method for the cloud analysis and the retrieved microphysical cloud properties will be given. Firstly, the data selection is explained, then the cloud property inversion retrieval algorithm, followed by the results and discussion.

3.1. Data selection

The lidar measured 24-hours a day and under all weather conditions. However, only a part of the data was appropriate for the cloud analysis. Various periods were manually selected for analysis based on the following criteria:

1. No precipitation was present
2. A single-layer stratocumulus cloud was present
3. The cloud had a clear visible cloud base

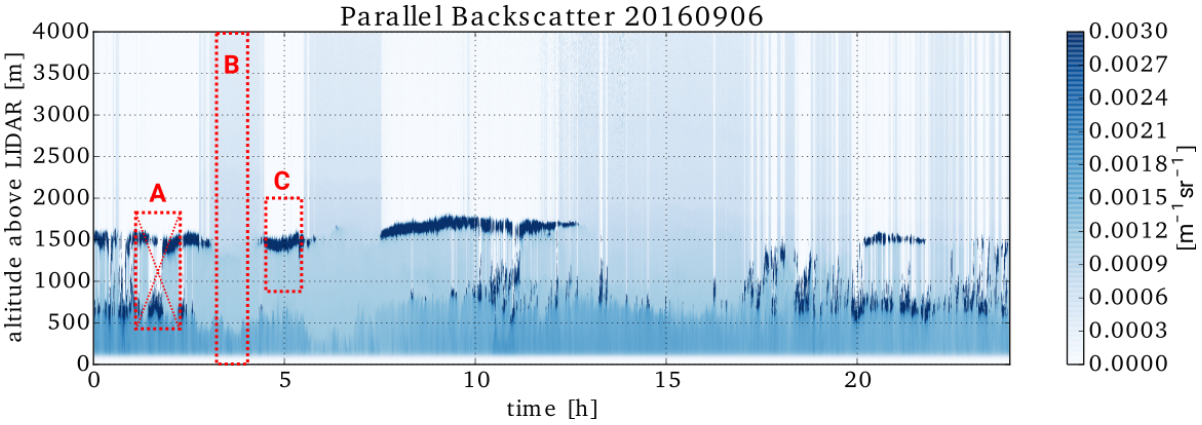

Figure 3.1: The parallel backscatter form the lidar for 06/09/2016. The red boxes show examples of selected data: A) a cloud with varying cloud base and double cloud layers, not appropriate for this analysis, B) appropriate selection of clear sky, C) appropriate selection of a cloud.

Figure 3.1 gives an example of the selection of the data. Box A displays cloud selection of a cloud with varying cloud base and double cloud layers, which is not appropriate for this analysis. Box B shows an appropriate selection of the clear sky (see also Chapter 4) and box C shows an appropriate cloud selection.

The selected parts of the data are listed in Table A.2 in Appendix. There were 43 cloud domains selected with a number of measurements varying between 5 and 298 (~ 2.5-149 minutes) per subset of the data.

3.2. Cloud property analysis

For each cloud selection the following cloud properties were computed: cloud effective radius (R_{eff}), cloud drop number density (ND), cloud extinction (α) and cloud base height (cbh). In order to obtain the cloud properties from the lidar signal the cloud property inversion retrieval algorithm of Donovan et al. [2015] was used. This method is developed for the UV-lidar and is based on the principles of multiple-scattering induced depolarization. An in depth explanation can be found in Donovan et al. [2015], here the method is summarized.

The inversion method used a simple cloud representation suitable for stratocumulus clouds [de Roode and Los, 2008], with a linear liquid water content profile and a constant cloud drop number density with height. Consequently, the cloud effective radius and the cloud extinction increased with height. For the cloud drop size distribution a single-mode modified gamma distribution was assumed [Mil]. With this model, the cloud can be described by just two parameters: the cloud effective radius and the cloud extinction at the reference height. A reference height at 100m above cloud base was used.

Lidar multiple scattering applied to this cloud model was simulated by Monte Carlo simulations using the model component of the Earth Clouds and Aerosol Radiation Explorer (EarthCARE) multi-instrument simulator software package. Several different input values of the cloud base height, lidar field of view, cloud effective radius and liquid water content lapse rate were modeled. The resulting attenuated parallel and perpendicular backscatter and the input parameters were stored in Look-Up-Tables (LUTS).

The inversion algorithm found a fit between those LUTS and the measured lidar signals. In order to do so, the peak altitude of each profile was shifted to the mean peak altitude, so the peak of each profile was at the same altitude. This is done to minimize the effects of cloud base changes within the averaging periods. A desired number of profiles were averaged, in order to get an estimate of the uncertainties from the standard deviation of the different profiles. Then the backscatter coefficients were normalized by:

$$B_{\parallel} = \frac{ATB_{\parallel}(z)}{max(ATB_{\parallel}(z))} \tag{3.1}$$

and

$$B_{\perp} = \frac{ATB_{\perp}(z)}{max(ATB_{\parallel}(z))}. \tag{3.2}$$

The normalization was done to remove variation associated with the (uncertain) absolute lidar calibration. After that a cost function was used to fit the normalized lidar observations with the LUTS. Therefore initial values of the cloud effective radius and the cloud extinction as well as the lidar constants were needed. The lidar constants were set to prior estimates (Table A.1 in Appendix), while the cloud effective radius and cloud extinction were obtained by an initialization procedure. In this initialization procedure a first fit of the LUTS profiles with the measured profiles was executed. Then by an iterative process the interpolated LUTS values were fitted through the measured values and when the cost function was minimized the final cloud effective radius and cloud extinction were retrieved. A covariance matrix was produced containing the errors of the fit. The cloud drop number density was calculated from the cloud effective radius and the cloud extinction,

$$N_0 = \alpha_{100} \frac{1}{2\pi} R_{eff,100}^{-2} \frac{1}{k}, \tag{3.3}$$

where k is 0.75+-0.15. The cloud base height was estimated from the LUTS backscatter profiles. For each variable the errors were calculated. However, this is done in the logarithmic domain, resulting in a different upper and lower uncertainty bound than in the linear domain. Uncertainties in the results are introduced by noise in the signal or by such factors as errors in the depolarization calibration factor or in the assumed k-value.

After the retrieval, one value for each cloud selection was obtained by calculating the weighted mean ($\bar{x}$) and standard error of the mean (σ_w) per cloud property for each selected cloud:

$$\bar{x} = \frac{\sum_{i=1}^{n} \frac{x_i}{\sigma_i^2}}{\sum_{i=1}^{n} \frac{1}{\sigma_i^2}}, \tag{3.4}$$

where n is the number of measurements in the selection, x are the values and σ are the upper error bounds of the values, and

$$\sigma_w = \sqrt{\frac{1}{\sum_{i=1}^{n} \frac{1}{\sigma_i^2}} * \frac{1}{(n-1)} * \sum_{i=1}^{n} \frac{(x_i - \bar{x}_i)^2}{\sigma_i^2}}, \tag{3.5}$$

where $\bar{x}$ is the weighted mean and n is the number of measurements in the selection.

3.3. Results

Figure 3.2A shows an example of the results of the depolarization based procedure. The data used was of a selected cloud of 06/09/2016. The left plot shows the normalized parallel attenuated backscatter coefficients observed by the lidar. The red line indicates 1 measurement, which is pointed out in the right side of the figure. The right side of the figure presents the fit of the retrieval (line) against the observations(dots). A good agreement is visible for the the parallel signal (∥) and the perpendicular signal (⊥). The cloud property fit parameters are shown in the right corner. The final cloud properties for this particular cloud selection are shown in Figure 3.2B. The shading shows the upper and lower error limits.

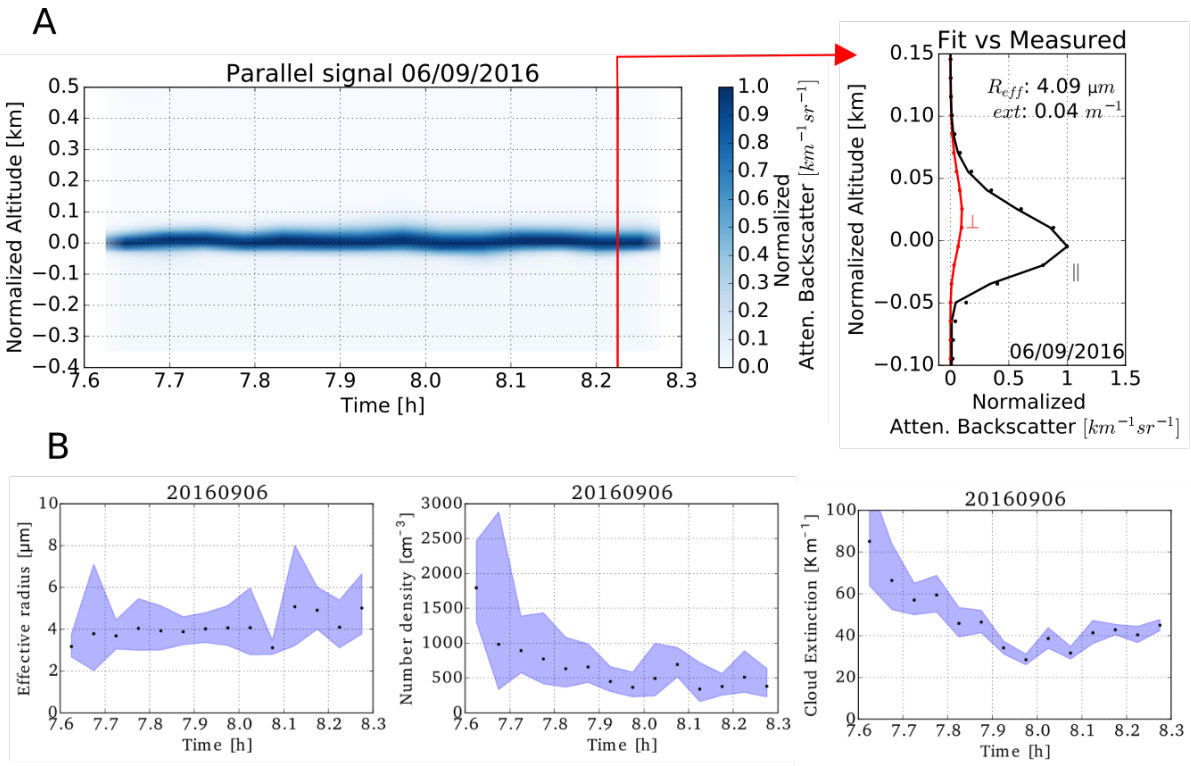

Figure 3.2: A) The lidar measurement (left) and the fit of the cloud inversion algorithm. The red line indicates one measurement. In the right figure the lidar measurement (dots) and the fit results(line) of the parallel attenuated backscatter (∥) and perpendicular attenuated backscatter (⊥) are shown. A good agreement between the measurement and the fit is visible. B) The final cloud properties -cloud effective radius, cloud drop number density and cloud extinction- from the selected cloud in A. The shading shows the upper and lower limits.

The weighted mean values of the retrieved cloud parameters for each selected cloud, as calculated using Eq. 3.4, are presented in Figure 3.3. In the first half of the month till 16th September the effective radius and the cloud base height were larger than in the clouds after 19th September. This division was less clear in the values of the cloud drop number density and the cloud extinction. The mean cloud effective radius varied between 1.88 and 4.48 μm. The cloud drop number density had values in the range of 228-1690 cm^{-3}. The minimum and the maximum of the cloud extinction is respectively 0.019 and 0.068 m^{-1} and of the cloud base height 760-1600 m.

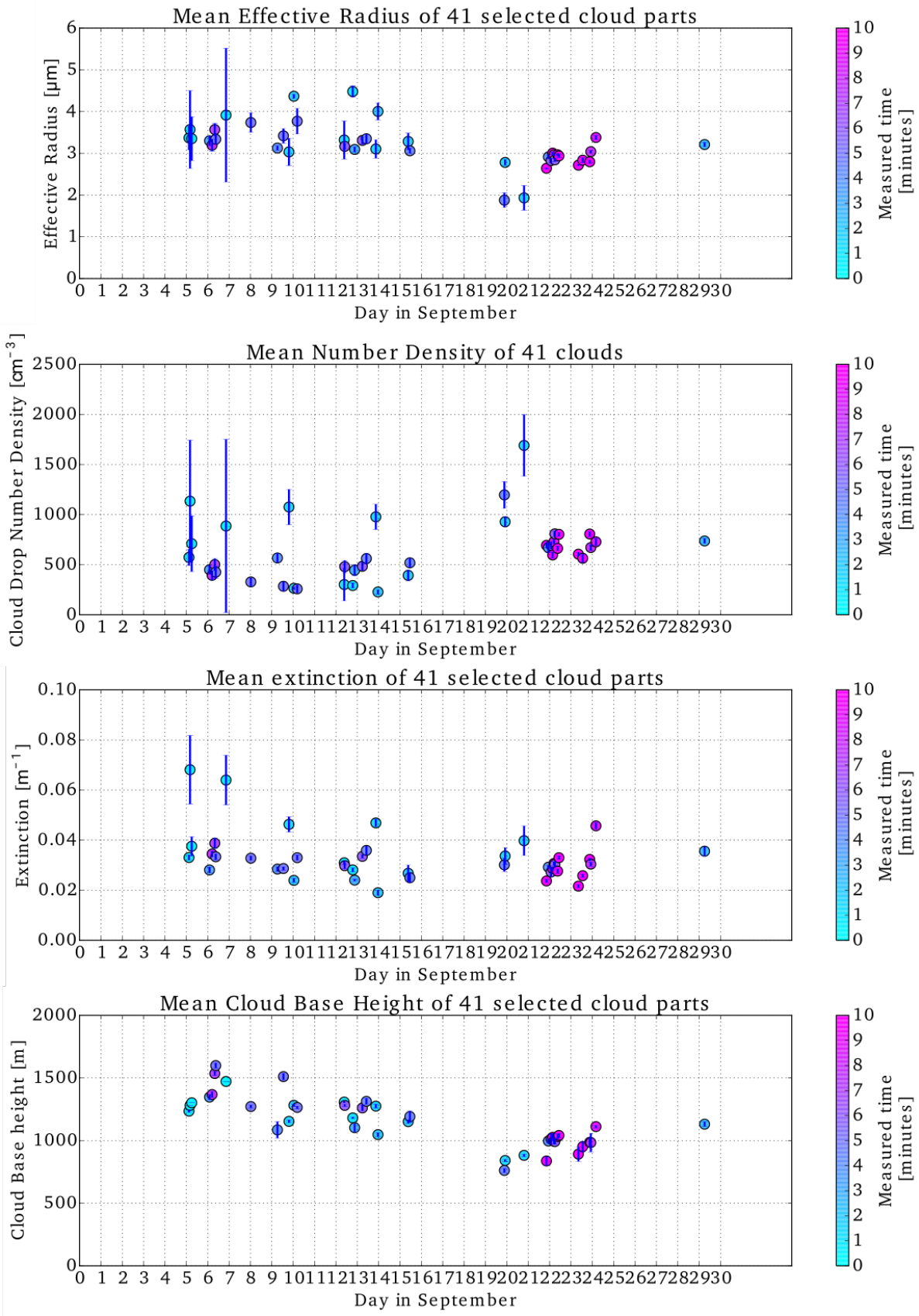

Figure 3.3: For each of the cloud selections the weighted mean and the standard error of the mean for the different cloud properties. The colors indicate the measurement time.

3.4. Discussion

When meteorological and aerosol conditions are similar we expect similar values of the cloud properties. In the month of September a shift in the cloud properties was visible, after the 19th of September lower effective radius and lower cloud base heights were observed. Therefore changes in meteorology (e.g. amount of water vapor, temperature, turbulence, dry air entrainment) or in aerosol loading should be considered as explanatory variables in future research. Also the period from 16 until 20 September could be investigated in future research, because those periods consisted double-layered clouds and rain events. Probably, during those periods the atmospheric conditions changed and by that the cloud formation altered.

The observed cloud properties are in the same range as we expected. The cloud effective radius was expected to be in the range of 1.9-13 μm and was found varying between 1.88-4.48 μm. Those radii can correspondent with a cloud drop number density around 1000 cm^{-3} and a liquid water content between 1 and 0.03 g/m^3. The observed cloud drop number density varied between 228 and 1690 cm^{-3}, which is high for marine air, but in the range of continental air. We did not investigate the liquid water content, which can be interesting to do in future research.

Previous ground-based remote sensing studies conducted at various locations have found cloud drop effective radii varying between 6-14 μm [Min and Harrison, 1996] and [Kim, 2003] (in Oklahoma) or between 3-8 μm [Sarna and Russchenberg, 2016] (on the Azores) and [Feingold et al.] (in Oklahoma). The type of the cloud and the type of the CCN determine the microphysical properties, so only research with similar conditions should be considered. In this case we found similar results for the cloud number density as Sarna and Russchenberg [2016] on the Azores. Although, the cloud drop effective radius in our study is smaller, while the measured altitude is 15m larger. Sarna and Russchenberg [2016] obtained the cloud properties at 85m above cloud base height, while we obtained at 100m above cloud base height. The droplets grow when ascending. Therefore it is reasonable to only consider the cloud number density. Sarna and Russchenberg [2016] found cloud drop number density in the range of 55-1900 μm, which is in the same order of magnitude as our results. The retrieval method used is recently validated by a new cloud property retrieval method developed by Rusli, which will be published in near future [personal contact, May 2017].

4

Aerosol profiles

In this chapter we explore the retrieval of aerosol profiles from the lidar measurements. First the aerosol profiles from clear sky scenes are retrieved. Those profiles were used to detect aerosol layers, from which the source was estimated by modeled back trajectories. Next, the aerosol profiles below the clouds are investigated. That is particularly interesting, because the aerosols below clouds are associated with the CCN and will affect the cloud formation more than aerosols higher in the atmosphere. However, to adjust the aerosol retrieval from clear skies to below clouds is challenging, because the cloud extinction is required and multiple scattering should be taken into account. Those problems are discussed in the last section.

4.1. Data selection

In order to examine the total aerosol loading only lidar measurements without clouds and/or precipitation should be considered, as shown in Figure 3.1. For the clear sky analysis, 29 periods were selected varying between 7 and 120 measurements (~3.5 and 60 minutes). The exact dates and times are reported in Table A.3 in the Appendix. For the aerosol profile retrieval below the clouds, the selected cloud parts were used as selected in Chapter 3.

4.2. Aerosol profiles - clear sky

For each clear sky selection the following aerosol profiles were obtained: aerosol extinction coefficient (α), aerosol scattering ratio (R_{ascat}) and aerosol backscatter coefficient (β). Those profiles were calculated based on the different contributions from the aerosols and the molecules on the lidar return signal. The lidar-equation (Eq. 2.2) can be combined with Eq.4.2 and Eq.2.4, whereby for a clear sky event the cloud part is equal to zero:

$$P(z) = \frac{C_{lid}}{z^2}(\beta_a(z) + \beta_m(z))e^{-2\int_0^z(\alpha_a(z')+\alpha_m(z'))dz'} \tag{4.1}$$

As we are interested in the aerosol component, the following steps were taken to obtain the aerosol extinction and backscatter from the lidar power. It is a boundary-value problem and can be solved following the approach of [Klett, 1984].

First Eq.4.1 is rewritten to a form like Eq.2.2:

$$P'(z) = \frac{C_{lid}}{z^2}\alpha'(z)e^{-2\int_0^z \alpha'(z')dz'}, \tag{4.2}$$

where

$$P'(z) = SP(z)e^{2\int_0^z \alpha_m(z')dz'}e^{-1\int_0^z S\beta_{m,\pi}(z')dz'} \tag{4.3}$$

and

$$\alpha'(z) = (\alpha_a(z) + S\beta_{m,\pi}(z)). \tag{4.4}$$

Eq.4.2 was used to calculate α':

$$\alpha'(z) = \left[\frac{\left(\frac{P'(z)z^2}{P'(z_0)z_0^2}\right)}{\frac{1}{\alpha'_0} + 2\int_z^{z_0} \left(\frac{P'(z)z^2}{P'(z_0)z_0^2}\right) dz'} \right], \tag{4.5}$$

where z_0 is the normalization height and α'_0 is the atmospheric extinction at normalization height.

From α' the aerosol extinction α and the aerosol backscatter β could be calculated using Eq.4.4 and Eq.2.13. The unknowns in this equation are the normalization height z_0, the extinction at normalization height α'_0 and the extinction-to-backscatter ratio S. The other variables can be obtained by either the lidar measurements or by the radiosonde measurements. The radiosondes measured the atmosphere above Ascension Island 8 times a day, although we interpolated those in time, it is the best information of the state of the atmosphere we had. If such measurements are not available, one could consider to use ECMWF forecast models. In our case we used the interpolated radiosondes as described in Section 2.3, to calculate the molecular contribution. At a normalization height of z_0 of 7000m we assumed there are no aerosols, so α_a can be neglected and α'_0 can be calculated from the molecular backscatter:

$$\alpha'_0 = S\beta_{m,\pi}(z). \tag{4.6}$$

The lidar power of this specific height is often very noisy. To reduce the noise averages over 5 range bins were calculated. The only unknown remaining is the extinction-to-backscatter ratio. This ratio depends on the aerosol type, properties and age. For aerosols at 355nm the value ranges from 17-75sr [Wandinger et al., 2016]. In this study a value of 50sr is used, which can be seen as valid for mixtures [Wandinger et al., 2016]. In order to validate the extinction-to-backscatter coefficient of 50sr, different extinction-to-backscatter ratios (40, 50 and 60) were tested, as shown in Figure 4.1, where the mean aerosol extinction profile from 20/09/2016 is given as an example. The larger this ratio, the higher the calculated aerosol extinction. This difference resulted in changes in the AOT(0-5000m), varying from 0.37 to 0.41 for a ratio of resp. 40 to 60sr.

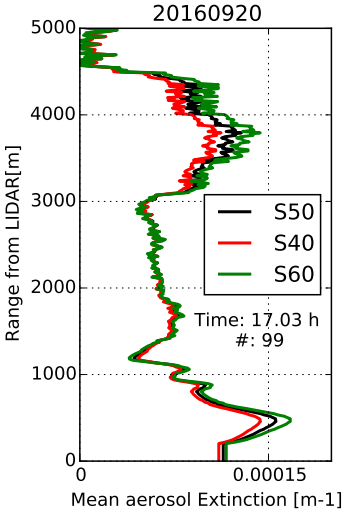

Figure 4.1: The mean aerosol extinction profiles from 20/09/2016 17h. The different colours indicate different values of the extinction-backscatter ratio. The larger this ratio, the higher is the aerosol extinction.

Nevertheless, information about the aerosol type is required in order to use the correct value for the extinction-to-backscatter ratio. The aerosol profiles does not provide that information. Therefore we used an atmospheric model, which provided backward trajectories of the air from a specific location and altitude, to investigate the aerosol sources. We used the Hybrid Single-Particle Lagrangian Integrated Trajectory (HYSPLIT) model [Stein et al., 2015]. The HYSPLIT model used the GDAS (1 degree, global, 2006-present) meteorology data in order to model the trajectory of the air backward in time. The backward trajectories were obtained till 10 days back.

Here we present the aerosol profiles from four days as examples (see figures in Figure 4.2). These days show different aerosol profiles. The profile from 07/09/2016 shows only aerosols in the lower part of the atmosphere till 1200 m and then a few aerosols around 2100 m. That is not the case for 15/09/2016, which

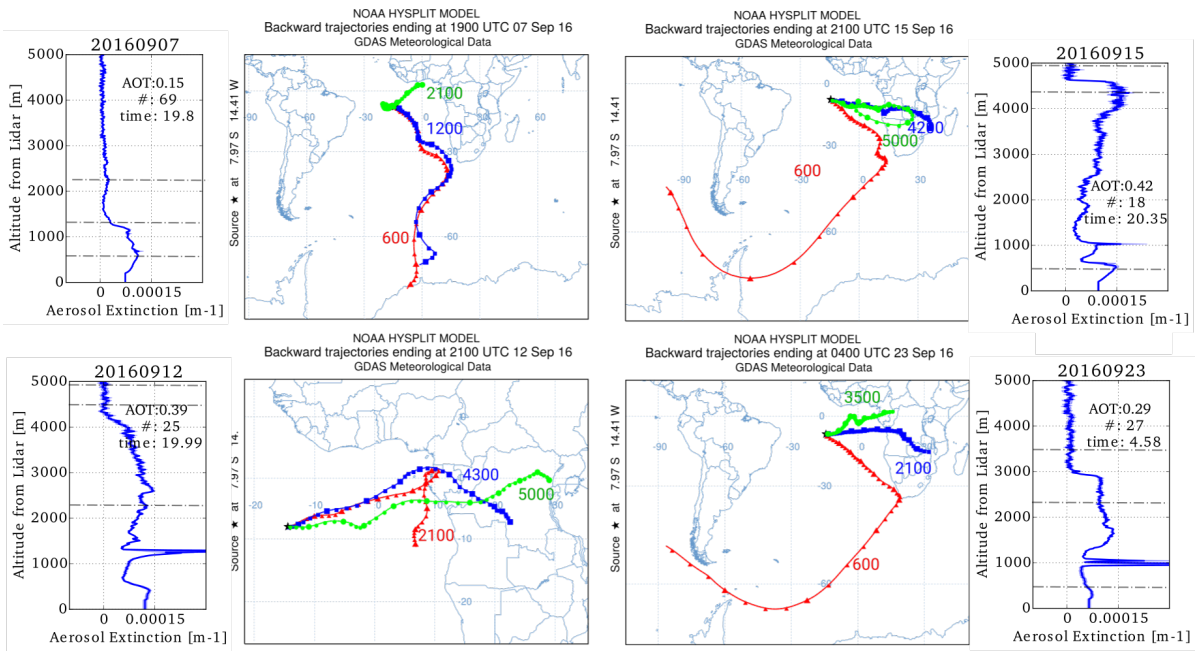

Figure 4.2: The figures at the left and right side show the daily-mean aerosol extinction coefficient profiles. Keep in mind that the error introduced by S of about 10% is not shown. The grey lines indicate the altitudes of interest for the HYSPLIT model. The center figures show the results of the HYSPLIT model.The different colored lines indicate the trajectory of the air arriving at Ascension Island (indicated by the star) at the noted altitude. These altitude were chosen based on the aerosol extinction coefficient profiles.

contained aerosols till an altitude of 4300 m. Noteworthy is the aerosol extinction peak at 4200 m, which gives a large aerosol return. The profiles from 12/09/2016 and 23/09/2016 also present a significant amount of aerosols, but does not show a peak at higher altitude. From those profiles, it is clear that the aerosol load changed per day. Besides the amount of aerosol extinction, the altitude of the aerosols changed, which could indicate different source locations. For each day three altitudes of interest were chosen to estimate the sources using the HYSPLIT model, as indicated in the figures of Figure 4.2 by the grey lines.

The backward trajectories for the four days are shown in the middle of Figure 4.2. The star indicates the final location of the air, in this case Ascension Island. In general the lower air (around 600 m) often arrived from the south being blown over the ocean. It is reasonable to assume that this air mainly contained marine aerosols. From 2100 m the air is directed from Africa. The air from Africa could contain smoke, depending on the presence of biomass burning events. The blue line (4300 m) at 15/09 contained a significant amount of aerosols, probably smoke particles. Also the air at 23/09 at 2100 m (blue line), directed from the same area, showed a peak in the aerosol extinction profile. In contrast, the air traveling from a northern area (23/09, green line 3500 m) did not show a peak in the extinction profile.

It could be concluded that the aerosols above Ascension Island have different source locations depending on time and altitude of the air mass, and that the backward trajectories give a global idea about the source, but more information is needed in order to distinguish between aerosol types. The backward trajectories showed the most probable path of the air, but cannot give any information about the composition of the air. Aircraft or ground-based in situ measurements are necessary to get this information.

4.3. Aerosol profiles - below cloud

For the aerosol retrieval below clouds a slightly different approach than described above is needed. It is the same boundary-value-problem, but the boundary value is set differently. In this case the normalization height is not located at an altitude without aerosols, but inside the cloud. In the cloud the contribution of the cloud particles is much larger than that of the aerosols and the molecules, so the latter could be neglected. The cloud base height and the cloud extinction are now crucial, they set the normalization altitude and the normalization extinction respectively. These values were obtained from the previously described cloud property inversion retrieval procedure. Besides that, the extinction-to-backscatter ratio should be taken differently inside the cloud than below the cloud, with a value of 20sr in the cloud and 50sr below the cloud [Wandinger et al., 2016]. Furthermore, multiple scattering, which influences the lidar return

and the cloud extinction, should be taken into account. In order to deal with this phenomenon the cloud extinction-to-backscatter ratio (S_c) is corrected:

$$S_c = \frac{(1-\eta)\alpha}{\beta}, \tag{4.7}$$

where η is the multiple scattering correction factor. Unfortunately, for technical reasons we could not obtain this factor from the cloud property inversion retrieval. In order to obtain a suitable approximation of the value, several test were done, whereby the aerosol profile from a clear sky moment is compared with the aerosol profile below cloud with different values of η. The results are presented in Figure 4.3 for the days 06/09/2016,10/09/2016 and 21/09/2016. The blue line is the clear sky profile, the green line the below cloud profile. A η value of 0.5 resulted in an overestimated aerosol extinction coefficient and a value of 0.3 in an underestimation. For the 21/09/2016 example a value of 0.35 showed the best fit, while the other days showed the best fit with a value of 0.4, as seen in the figures in the red boxes. The difference in aerosol extinction coefficient at an altitude of 300 m below cloud base between η = 0.35 and η = 0.4 is about $2.6 * 10^{-5} m^{-1}$. We used for all clouds a value of 0.4 for the data processing.

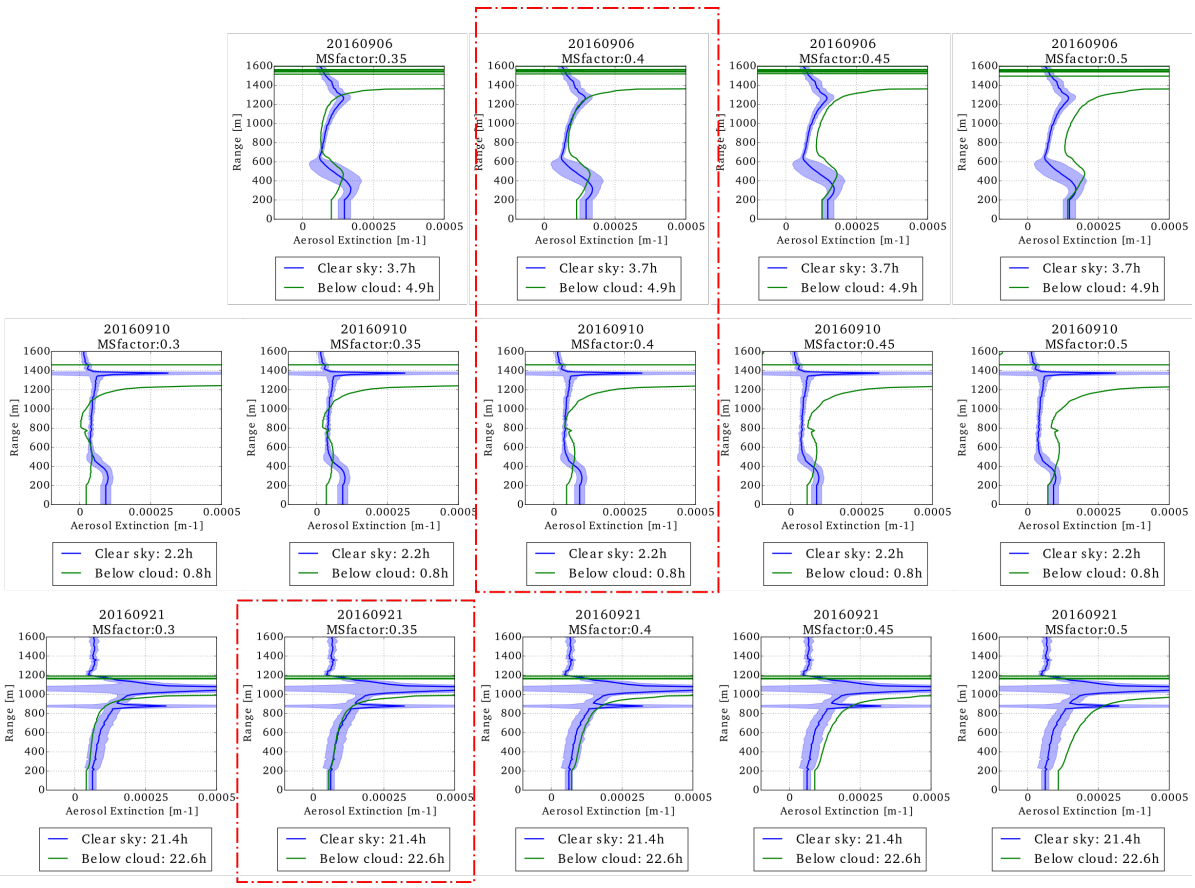

Figure 4.3: Test results of the aerosol extinction coefficient profiles below cloud (green line) versus the mean profiles at clear sky moments (blue line, with standard deviation in shaded area. Keep in mind that the error introduced by S of about 10% is not included.) for different multiple scattering factors (η). The horizontally sequenced figures are from the same day and time. The vertically sequenced figures have the same η. The red boxes indicates the best fit. For each of those below cloud cases the aerosol extinction coefficient is compared with the aerosol extinction coefficient from a clear sky moment close in time. We used for all clouds a value of (η) 0.4 for the processing.

4.4. Results

For each of the clear sky selections an aerosol extinction coefficient profile was made. Although the aerosol profiles differ between different days, the aerosol load does not seem to change much within one day. Therefore the aerosol selections were combined to one profile per day, see Figure 4.6. Only for the 10th of September an exception was made, because after 20 h a higher aerosol layer seems to appear, Figure 4.4. So for this

day two profiles were made. Those daily mean aerosol extinction coefficient profiles were used in the investigation of the aerosol-cloud interaction. Besides the clear sky profiles, the aerosol extinction profiles of the below cloud parts were obtained. For those profiles the mean aerosol extinction coefficient below clouds were calculated as shown in Figure 4.5. The mean aerosol extinction coefficient was calculated for the range 200m above the lidar till 300m below the cbh. This range was chosen to avoid the lidar overlap region and the mixing region of wet aerosol just below the cloud base. The error bars show the sample standard deviation of each cloud selection, without taking into account errors in S and η. The colors indicate the amount of measurements were included, whereby the pinker the color, the more measurements.

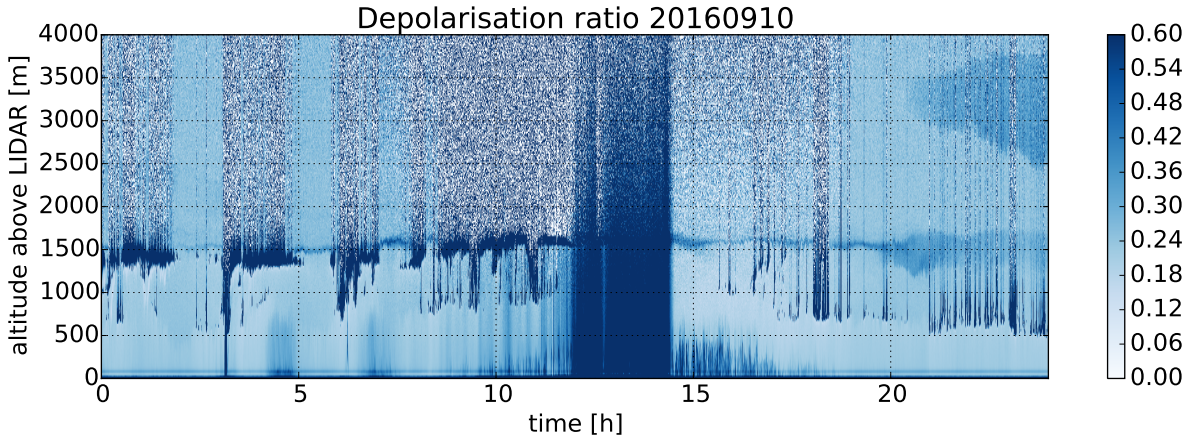

Figure 4.4: The lidar depolarization ratio of 10/09/2016. After 20:00h an aerosol layer at 3500 m appeared.

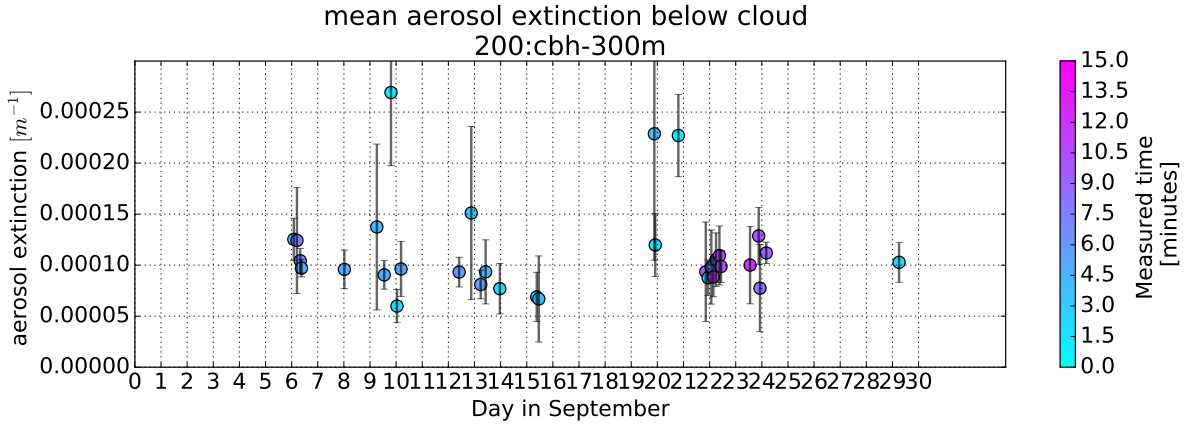

Figure 4.5: The mean aerosol extinction and standard deviation from the range 200:cbh-300m for each selected cloud. The aerosol extinction profiles from below cloud were used. The colors indicate the measured time from the selection. The error bars show the sample standard deviation of each cloud selection, without taking into account errors in S and η.

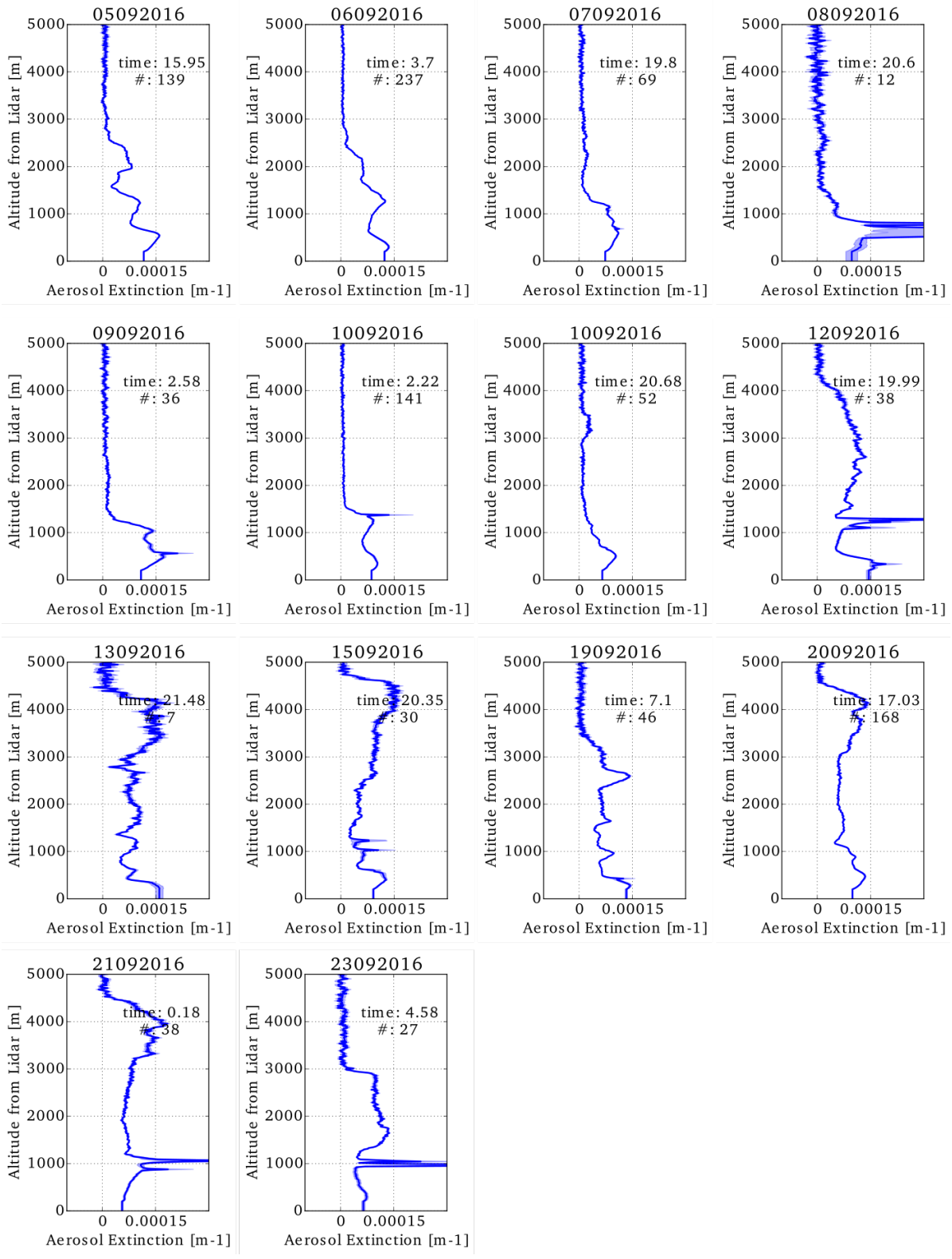

Figure 4.6: The daily mean aerosol profiles obtained by the aerosol algorithm described above. The shaded areas only includes the variation of the obtained profiles, no other errors such as the errors in S are included.

4.5. Discussion

In this chapter we retrieved the aerosol profiles for clear sky cases and below the clouds. Although the profiles showed a reliable structure, some potential issues should be mentioned. The algorithm used a single extinction-to-backscatter ratio for atmosphere without clouds. However, considering the different aerosol sources, different ratios for different layers could give a better result, because the extinction-to-backscatter ratio S depends on the properties of the aerosols. In our case we assumed a value of 50sr, which is reasonable for forest fire smoke aerosols and mixtures, but too high for marine aerosols, which would be around 25sr [Müller et al., 2007]. An increase in S of 20sr, from a value of 40 to 60, led to a change of 0.04 in AOT. A better understanding of the aerosol types would increase the reliability of the aerosol profiles and the AOT. However, the structure of the profile would not change by altering the ratio S, therefore an error in the ratio S would not propagate through to the aerosol-cloud interaction calculations.

The backward trajectories provided some information on the source of the aerosols; the lower part of the atmosphere (0-1200m) often came from the south over the ocean, while the higher air could arrive from the East from the African continent. It would not be surprising if both air volumes contained totally different types of aerosols. The lower part could contain more marine particles, and the upper part more smoke particles. Nevertheless, in situ measurements are needed to investigate this in detail. Another option is the use of Raman lidar or high spectral resolution lidar. Those instruments can measure the extinction-to-backscatter ratio directly [Ansmann and Muller, 2005]. When that knowledge is available, different layers could be inserted in the aerosol profile retrieval algorithm and the difference in aerosol type (and in S) could be taken into account. Additionally, the origin of the air could be checked by forward trajectories from the biomass burning events.

Furthermore, the aerosol retrieval below clouds provided already a two-layered approach, whereby a different ratio is used inside the cloud than below the cloud. Such an approach can be developed for the clear sky cases too. First an initial quess can be obtained by the single-layered version. Then the peaks can be used for the backward trajectories, which will provide some information about the aerosol source. After that, different ratios can be considered and an updated profile can be retrieved. However, backward trajectories are still models, which does not provide detailed information about the aerosol properties at a certain location. Be careful if no detailed information is available, because such an differentiation in S will change the aerosol extinction profile, hence will change the AOT and the further calculations on the aerosol cloud interactions.

Besides the extinction-to-backscatter ratio, the multiple scattering factor on the extinction-to-backscatter ratio inside the cloud introduces uncertainties. A cloud generates multiple scattering which result in underestimated extinction coefficients measured by the lidar. This was accounted for by introducing a multiple scattering factor. In this research we used the aerosol extinction profiles of a clear sky close to a cloud to correct the profiles below a cloud and to choose a multiple scattering factor. For the 3 tested cases this factor was between 0.35-0.4, with a difference of $2.6 * 10^{-5} m^{-1}$ in the extinction at 300m below cloud base. This multiple scattering factor is in the same range as found by Platt [1980]. Nonetheless, it is impossible to check the ratio for each selected cloud with a clear sky moment, simply because that is not always available. A more accurate method would be to use the Monte-Carlo simulations made for the cloud property inversion retrieval algorithm and calculate the ratio between single and multiple scattering. That will result in a specific factor for each cloud selection, independent from the clear sky analysis.

5

Aerosol-Cloud Interactions

Until here we retrieved the cloud properties and the aerosol profiles separately for parts of the data set. Now we can combine those in order to examine the aerosol-cloud interactions and to obtain the cloud properties as a function of aerosol loading. As discussed in the introduction, the aerosol loading can have several influences on clouds. We focused on the indirect effect and specifically the Twomey effect. Thus the question to answer is: when there is an increase in aerosol loading, will that result in an increase in cloud drop number density and a decrease in cloud effective radius? Three different approaches are explained, see Figure 5.2. First a coarse classification was done by averaging the data into 3 categories: 'clean', 'mixed' and 'separated', for respectively few aerosols, aerosols at cloud level and aerosols distinctly above the cloud level. Secondly, the Indirect Effect quantity (IE) was determined for the total month, whereby the mean AOT per day was used as aerosol proxy. Thirdly, for each individual cloud selection the IE quantity was obtained, whereby the mean extinction coefficient below cloud was used as aerosol proxy.

5.1. Approach 1: classification

This approach created a classification, which is based on a previous research [Brown, 2016]. Brown [2016] made a classification of aerosol content per day based on the depolarization ratio of the lidar measurements from the same data set as used here. The categories were; 'clean' whereby no aerosol layer was clearly visible, 'mixed' whereby the aerosol layer exist at about the same height as the cloud and 'separated' whereby is assumed that the aerosol layer is above the cloud separately from the cloud, see Figure 5.1B. This classification was done by eye. Then the clouds were divided per category and per cloud property the mean value was calculated. The aerosol-cloud interactions were discussed by comparing the 'clean' and 'mixed' category.

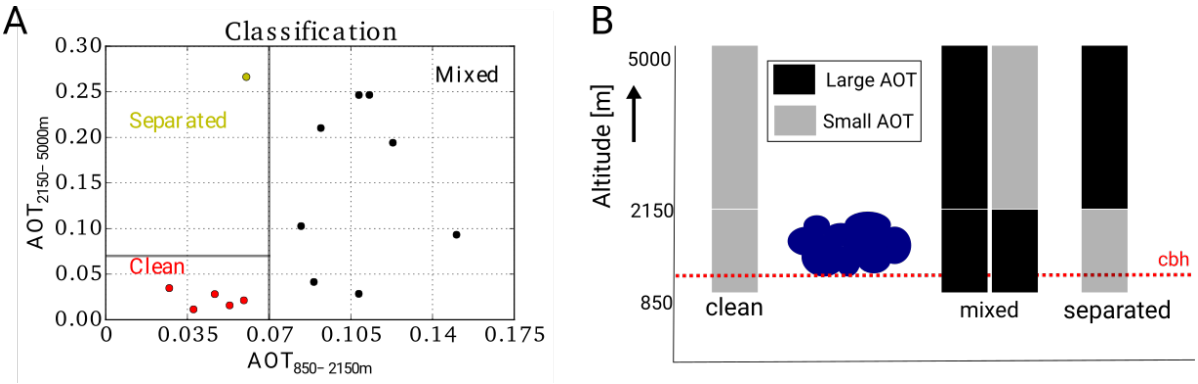

Figure 5.1: Explanation of the classification approach. A)The data from the daily mean aerosol selections for the different two AOTs; namely from 850-2150m (x-ax) to indicate the air at the cloud layer and from 2150-5000m (y-ax) to indicate the air above the cloud layer. The data is divided into three categories: clean, mixed and separated. B) Illustration of the classification. The boxes show the area of the AOT, while the grayness the amount of aerosols indicates.

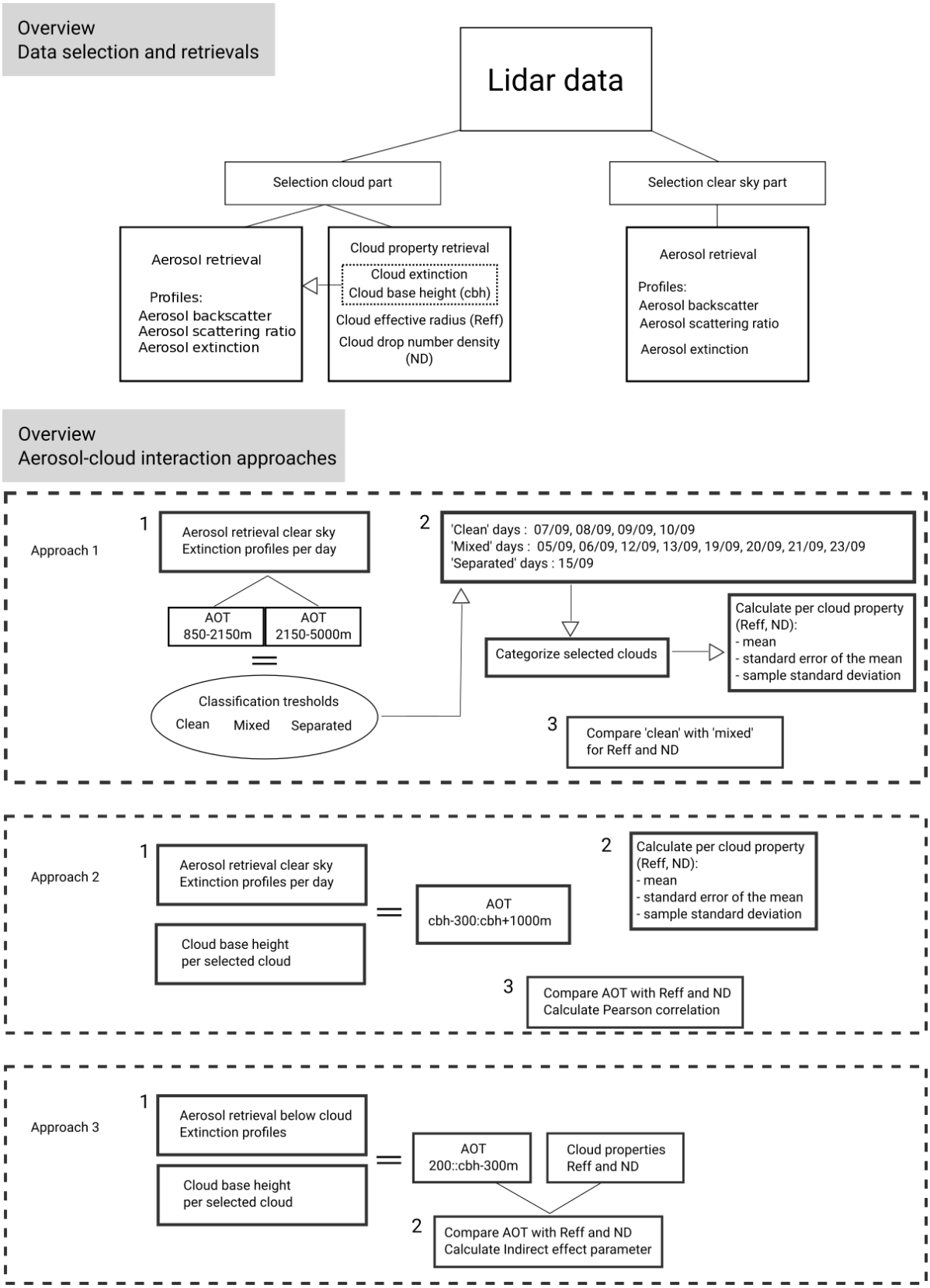

Figure 5.2: Overview of the data selection steps and retrieval (upper part) and an overview of the aerosol-cloud interaction approaches (lower part). The data used and processing steps are set out.

In the project presented here the mean aerosol profiles from clear skies of each day were used. The process could be divided into three different steps (Figure 5.2). First for each profile two different AOT values were calculated (Eq.2.9). One at cloud level, which is the cloud level in case clouds are present, whereby the boundaries were chosen from 850-2150m, the other above the cloud level up to 5000m, Figure 5.1B. Then Figure 5.1A was produced. From this figure three different classes were made. The first classification rule was based on the $AOT_{850-2150m}$, whereby the value of 0.07 was chosen by eye. The second classification rule based on the other AOT was arbitrary chosen close to the group of measurements called 'clean'. The classification rules were set:

- 'Clean' : $AOT_{850-2150} < 0.07$ & $AOT_{2150-5000} < 0.07$
- 'Mixed' : $AOT_{850-2150} > 0.07$
- 'Separated' : $AOT_{850-2150} < 0.07$ & $AOT_{2150-5000} > 0.07$

Secondly, for each day the mean aerosol profile from clear skies was used to classify that day, leading to the following days per category:

- 'Clean' days : 07/09, 08/09, 09/09, 10/09
- 'Mixed' days : 05/09, 06/09, 12/09, 13/09, 19/09, 20/09, 21/09, 23/09
- 'Separated' days : 15/09

Brown [2016] classified the days slightly different, the 10th of September was not a 'clean' day but a 'separated' case. Furthermore, Brown classified all the measured days, while we only considered the days from which we could obtain cloud properties.

After the classification of the days, the selected cloud data was clustered per category. So all the selected clouds at the days of the category 'clean' were grouped. In principle only the days of which we got clear sky scenes and single-layered non-precipitating cloud were encountered. One exception was the 22/09/2016, which did not have any clear sky scene. This day was classified as 'mixed', because the 21^{th} and 23^{rd} were in that category. For each category the weighted mean, the standard error of the mean and the sample standard deviation for the cloud drop effective radius and number density were calculated. For those calculations Eq.3.4 and Eq.3.5 were used with the weighted mean and standard error of the mean as obtained in Chapter 3 for resp. x and σ and for n the number of clouds in the category.

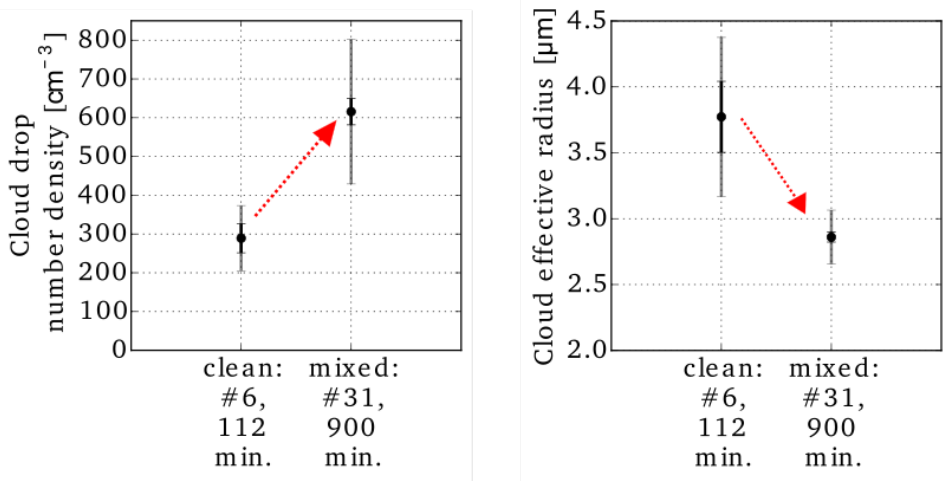

Figure 5.3: The mean value of the cloud drop number density (left) and the cloud effective radius (right) per category. The black error bars represent the standard error of the mean, the grey bars the sample standard deviation. The arrows indicate the influence of the increase of aerosols from a clean to mixed atmosphere, so an increase in cloud drop number density and a decrease in effective radius.

Thirdly, the weighted mean values of the 'clean' and 'mixed' cases were compared in order to investigate the influence of aerosols upon the clouds, as in Figure 5.3. The mixed category showed a higher number density, while the effective radius dropped in comparison with the clean category. The error bars of the standard error of the mean as well as the sample standard deviation do not overlap for the clean category compared to the mixed category, thus there can be concluded that the mean values are significantly different.

5.2. Approach 2: clouds compared with clear sky aerosols

The next approach is comparable with the previous, in such that the cloud properties were linked to a specific day and to a daily mean clear sky aerosol profile. However the aerosol profiles were not used to define categories, but were directly compared with the cloud properties via the AOT. First for each selected cloud the aerosol profile of that particular day was used to calculate the AOT. The boundaries of the AOT were chosen to be 300 meter below the cloud base (z_1) till 1000 m above cloud base (z_2). This part of the atmosphere was assumed to have a role in the cloud formation, because the aerosols within this part probably react as CCN. For the cloud properties the weighted means are used, as obtained in Chapter 3.

The last step was to investigate the relation between cloud properties - effective radius and cloud drop number density - and the AOT using the Indirect Effect parameter (IE, Eq.2.11 and Eq.2.12), see results in Figure 5.6. Each dot represents one cloud selection. The black error bars give the standard error of the mean and the dashed line shows a linear fit of the logarithmic values. The errors were taken into account as weights in the linear fit method. The cloud drop number density versus the AOT got a positive IE value of 0.3±0.21, while the IE for cloud effective radius had a negative value of -0.18±0.06. The sign of the IE quantities is consistent with the Twomey effect, because the cloud drop number concentration increased with increasing AOT and the cloud effective radius decreased.

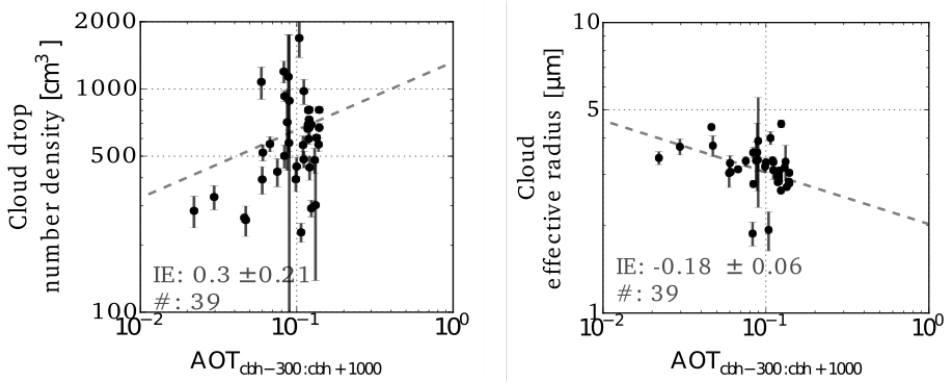

Figure 5.4: Left: The weighted mean cloud drop number density versus the AOT for each cloud selection. Right: The weighted mean cloud effective radius versus the AOT for each cloud selection. For both cloud properties a linear fit is plotted and the Indirect Effect parameter (IE) is given. During the linear fit the standard error of the mean values were used as weights.

5.3. Approach 3: clouds compared with below cloud aerosols

The last approach is different from the previous ones, because the aerosol profiles clear sky were not considered. The aerosol loading was determined using the aerosol profiles below the cloud. Firstly, for each selected cloud the mean aerosol extinction coefficient was calculated from the aerosol extinction profile below that cloud (200m above the lidar till z_2 300m below the cloud base height). This range was chosen to avoid the lidar overlap region and the mixing region of wet aerosols just below the cloud base. The mean aerosol extinction coefficient was used in stead of the AOT, because the height of the range bins altered per cloud selection. Secondly, the aerosol-cloud interactions were expressed with the Indirect Effect parameter (IE), whereby cloud selections with less than 3 data values were excluded. For the cloud properties the individual retrieved values were used, not the weighted mean values. The upper errors obtained by the cloud property inversion retrieval algorithm were used as weights to determine the IE values.

The resulted IE_r and IE_N for each selected clouds can be found in Figure 5.5, and in Table A.4 in the Appendix. The IE_r got values in the range from -1.27 to 0.79 and for IE_N between -1.40 and 3.19. The number of measurements taken into account varied between 3 and 24, which corresponded with a measurement period of 1.5 till 12 minutes. If we focus on IE_N, then some of the clouds show a positive value. A positive value means an increase in cloud number density with an increase in aerosol loading. That is an evidence for the Twomey effect. Some of the values are around zero, which can be interpreted as an altering in cloud property probably caused by other processes than the aerosol loading. During such period the change in aerosol did not cause a change in cloud property. Only a few cloud parts show a negative IE_N value, which also indicates different processes than aerosol loading effects. A negative IE value suggest that the cloud number density decreased with increasing aerosol loading. Therefore other processes should be investigated,

such as dry air entrainment and changes in humidity over time. Moreover, the values are large in comparison with the theoretical physical numbers. The IE_r could not exceed the 0.33, while the IE_N should be below the 1.0 (the grey lines in Figure 5.5). Although, some of the 'non-theoretical-supported' IE values are associated with large error bounds. Those limits are base on theoretical clouds, whereby among other things a constant state of the atmosphere is assumed. In practice the state of the atmosphere is variable, so those changes should be included. Those changes are beyond the scope of this project. We advise to investigate the errors and to include the meteorological variation in future research.

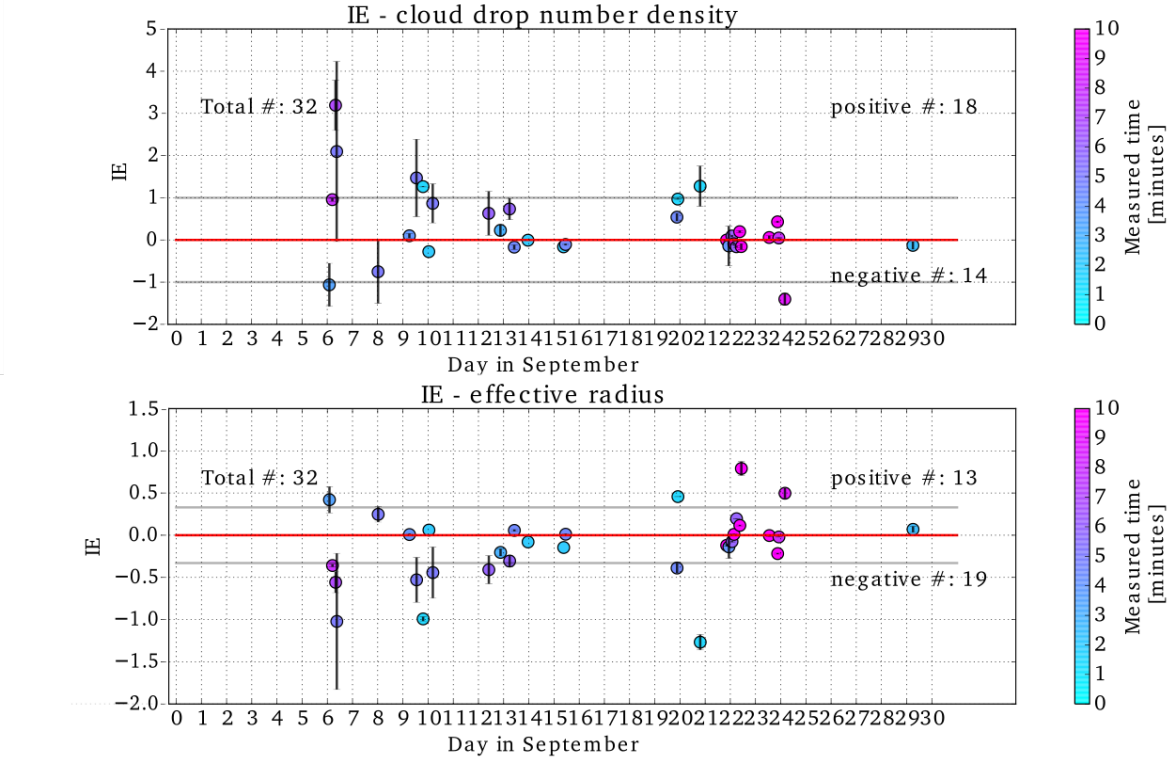

Figure 5.5: Each dot represents the IE for a selected cloud. For the aerosol proxy the mean aerosol extinction of the region below the cloud was used. For the cloud property was the property used as obtained by the cloud property inversion retrieval algorithm.The upper errors obtained by the cloud property inversion retrieval algorithm were used as weights to determine the IE values. The colors indicate the measurement time.

5.4. Discussion

To summarize, three different approaches to investigate the aerosol-cloud interactions were investigated. Each approach showed evidence for the Twomey effect. Nevertheless some discussion points needs to be mentioned.

Overall, the data selection is crucial. For some days several cloud periods were selected, while other days had only one possible cloud. Also the duration of the selected cloud was variable. Therefore, the mean cloud properties as in approach 1 could be dependent on just a couple of days. Perhaps a better approach would be a fixed time period per cloud selection, and a fixed number of selection per day. That can be very challenging, because the weather (including clouds) is very variable and non-uniform.

Related to data selection is the variability within each selection. In order to observe aerosol-cloud interactions variation in aerosol proxy and in the cloud properties is required. If only small variation in one of them is observed, reliable IE parameters cannot be retrieved. In Figure 5.6A, the variation in aerosol proxy and in the cloud parameters are small. Therefore those results should be considered with care, which is already noted by the unrealistic value calculated in IE. For the cloud drop number density the calculated IE had a value of -0.16 with an uncertainty of 0.27. The selected cloud could have had a time period too short to observe variation, or other effects interfered, such as changes in LWP.

Other points of interest are the meteorological effects, such as changes in LWP. The Twomey effect exist only when the LWP is constant, otherwise changes in LWP might have caused the changes in the cloud prop-

erties. However, in this research this information was not available, thus we assumed constant LWP. Besides that we assumed that the state of the atmosphere was comparable during the measurement period. So the clouds observed at different days could be combined as in the first and second approach. The last approach solved that problem by taking each cloud selection individual. Nevertheless, the theoretical IE values were exceeded, but some of those are associated with large uncertainties. Therefore, a better knowledge of the meteorology could help in describing the aerosol influences, because cloud formation does not only depend on the aerosols. For that reason, we suggest further research on this to answer the questions: How do the meteorological factors change during the measurement period? How do the meteorological factors contribute to cloud formation? Where we mean the LWP, turbulence, temperature and water vapor content as meteorological factors.

Furthermore, the aerosol proxy was different per approach. The first two approaches compared the aerosol information from clear sky scenes with the cloud properties. Per day one mean profile was considered. The last approach used only the aerosol layer below the cloud base. Nonetheless, the location of the aerosol layer with respect to the cloud is besides the amount of aerosols and the aerosol type important to take into account. As shown in the modeled back trajectories the type of the aerosols changes per altitude depending on the source. Different aerosols have a different effect on the atmosphere. Therefore we suggest for further research to investigate the location of the aerosol layer and the possible interactions with the cloud, so the correct aerosol layer are linked with the clouds. To which degree play the aerosol below the cloud, at cloud base height and above the cloud a role in the cloud formation?

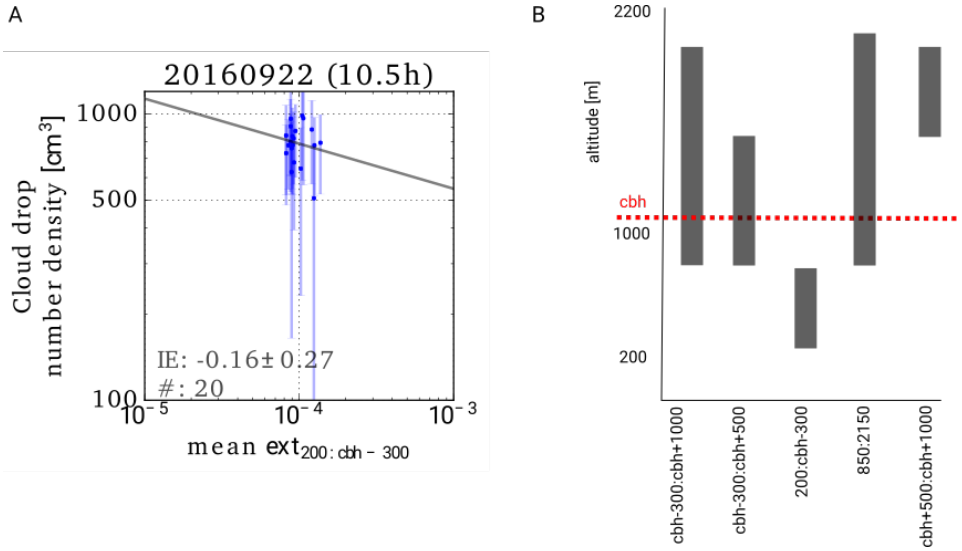

Figure 5.6: A) The IE value for the selected cloud at 22/09/2016 around 10.5h. The variation of aerosol extinction is small causing large uncertainty in the IE value. B)Illustration of the different altitude ranges used for determining the influence of different layers on the clouds.

Table 5.1: The resulted IE values for different aerosol layers with the cloud properties - IE_r for cloud effective radius and IE_N for cloud drop number density- and their uncertainty. For the cloud proxy the mean aerosol extinction is used.

lower bound [m]	upper bound [m]	IE_r	IE_N	#
cbh-300	cbh+1000	-0.15 ± 0.05	0.25 ± 0.18	39
cbh-300	cbh+500	-0.15 ± 0.06	0.34 ± 0.21	39
200	cbh-300	0.02 ± 0.11	0.67 ± 0.29	39
850	2150	-0.13 ± 0.05	0.18 ± 0.19	39
cbh+500	cbh+1000	-0.1 ± 0.03	0.15 ± 0.12	39

We did already a small test to explore this, see results in Table 5.4 and the used boundaries in Figure 5.6B. The same procedure as in approach 2 was used, only the mean aerosol extinction coefficient instead of the AOT was used in the calculation of IE. Otherwise the AOT calculated for height of the bin in the range 200:cbh-300m was variable due to variation in the cbh. If we focus on the IE_N, the air layer below the cloud between 200:cbh-300m got the highest IE_N value. This is in line with the theory that the aerosols below the cloud can be connected to the cloud base and may have an influence on cloud formation,while the influence of aerosols above the cloud will be smaller [Hegg et al., 2012]. The IE_N values from the other altitude ranges showed a smaller Twomey effect. Related to the aerosol layers is the decision made for the classification in approach 1. We based the classification rules on the $AOT_{850-2150}$ and $AOT_{2150-5000}$, however different boundaries of the AOT will result in different AOT values and maybe in different classification rules. Nevertheless, the result of the classification was the same as in previous research ([Brown, 2016]). Different boundaries could be chosen, if other layers seem more reasonable for the aerosol cloud interactions.

Furthermore, from the back trajectories might be assumed that the lower part of the atmosphere (0-1200m) mainly contained marine aerosols, which is probably not linked with the African smoke. In order to distinguish between marine and smoke aerosols in situ measurements are needed. Future research should focus on the cloud formation mechanics in combination with the influence of different aerosol layers.

6

Conclusion

The focus of this research was on the investigation of aerosol-cloud interactions above Ascension Island. Furthermore the only measurements considered were measured by the UV-lidar. We showed that it is possible to obtain the cloud properties -cloud effective radius, cloud drop number density, cloud extinction and cloud base height- from single-layered non-precipitating clouds using the lidar measurements only. Besides the cloud properties, aerosol extinction profiles for clear sky scenes as well as profiles below the clouds were derived. Those profiles showed the structure of the aerosol loading, which could be used to get the aerosol source from modeled backward trajectories. Moreover, the aerosol optical depth for the total column and for different altitudes could be calculated. Then the aerosol optical depths and the cloud properties could be used together in order to examine the aerosol-cloud interactions. Three different approaches were studied to determine if the Twomey effect occurred. The theory of the Twomey effect predicts that an increase in aerosol loading results in a decrease in cloud effective radius and an increase in cloud drop number density under constant liquid water path conditions. Although the liquid water path was not known, all of the approaches gave evidence for the Twomey effect.

Further research should be done on the location dependency of the aerosol loading with respect to the cloud locations and its influence on the aerosol-cloud interactions. The approaches discussed in this report could be extended using different AOT boundaries, which is possible because the total aerosol profile is known. Moreover, the Twomey effect is only stated from the sign difference in the Indirect Effect quantity. However, a more statistical analysis could give an answer on the questions 'to which extent the aerosols influenced the clouds?' and 'which percentage of the change in cloud properties is caused by changes in aerosol loading?'. Also other atmospheric parameters (e.g. the liquid water path and turbulence) needs to be considered and their influence on the cloud formation should be studied. Also the clouds itself, their formation and type, needs to be studied to give a broader overview of the system.

Besides that, a further study on the sources of the aerosols could be done using the back ward trajectories but also include forward trajectories of known biomass burning events. The knowledge of the source provide information of the aerosol type, which could be use to validate and to improve the aerosol profile retrievals. Additionally, the cloud properties and the aerosol profiles should be further validated by other techniques, using in-situ or other remote sensing measurements. That increases the confidence in the retrieval algorithm results of the retrieval algorithms and will strengthen the results of this project. Those results can then be used to validate climate change models and improve those models. Especially, when more knowledge about the aerosol-cloud interactions is gained using this measurement technique in future research projects.

Acknowledgment

I would like thank Dave Donovan for all the help and knowledge about the lidar and the retrieval algorithms. It was really encouraging and inspiring to discuss the project. The same is true for the meetings with Martin de Graaf. We could discuss about the measurements and what to study next. Then I like to thank Herman Russchenberg for the scientific interest and discussions. I thank Deborah Stein-Zweers for her interest in the biomass burning processes and backward trajectories. I acknowledge Jessica Brown for setting up the measurements. Mark Lammers thanks for the suggestions for data analysis and statistics. Lastly I would like to acknowledge some data sources: data were obtained from the Atmospheric Radiation Measurement (ARM) Climate Research Facility, a U.S. Department of Energy Office of Science user facility sponsored by the Office of Biological and Environmental Research; from Copernicus Atmospheric Monitoring (CAMS); the NOAA Air Resources Laboratory (ARL) for the provision of the HYSPLIT transport and dispersion model.

Bibliography

EZ aerosol and cloud lidar, user's manual, 2007.

V Amiridis, D S Balis, E Giannakaki, A Stohl, S Kazadzis, M E Koukouli, and P Zanis. Optical characteristics of biomass burning aerosols over Southeastern Europe determined from UV-Raman lidar measurements. *Atmos. Chem. Phys. Atmospheric Chemistry and Physics*, 9:2431–2440, 2009. URL www.atmos-chem-phys.net/9/2431/2009/.

Albert Ansmann and Detlef Muller. *Lidar and atmospheric aerosol particles*. Springer, 2005. ISBN 0-387-40075-3.

D. Randall P. Artaxo C. Bretherton G. Feingold P. Forster V.-M. Kerminen Y. Kondo H. Liao U. Lohmann P. Rasch S.K. Satheesh S. Sherwood B. Stevens Boucher, O. and X.Y. Zhang. Clouds and aerosols. in: Climate change 2013: The physical science basis. 2013.

J Brioude, O R Cooper, G Feingold, M Trainer, S R Freitas, D Kowal, J K Ayers, E Prins, P Minnis, S A Mckeen, G J Frost, and E.-Y Hsie. Effect of biomass burning on marine stratocumulus clouds off the California coast. *Atmos. Chem. Phys. Atmospheric Chemistry and Physics*, 9:8841–8856, 2009. URL www.atmos-chem-phys.net/9/8841/2009/.

J Brown. Inverting ground-based polarisation lidar measurements to retrieve cloud microphysical properties during the ascension island initiative, 2016. URL http://bibliotheek.knmi.nl/knmipubIR/IR2016-10.pdf.

R.T.H Collis and P.B. Russell. Lidar measurement of particles and gases by elastic backscattering and differential absorption. In *Laser monitoring of the atmosphere*. Springer-Verlag, 1976.

M. de Graaf, L.G. Tilstra, P. Wang, and P. Stammes. Retrieval of the aerosol direct radiative effect over clouds from spaceborne spectrometry. *Journal of geophysical research*, 2012. doi: 10.1029/2011JD017160.

M. de Graaf, N. bellouin, L.G. Tilstra, and P. Haywood, J.and Stammes. Aerosol direct radiative effect of smoke over clouds over the southeast atlantic ocean from 2006 to 2009. *Geophysical Research letters*, 2014. doi: 10.1002/2014GL061103.

Stephan R. de Roode and Alexander Los. The effect of temperature and humidity fluctuations on the liquid water path of non-precipitating closed-cell stratocumulus clouds. *Quarterly Journal of the Royal Meteorological Society*, 134(631):403–416, 2008. ISSN 1477-870X. doi: 10.1002/qj.222. URL http://dx.doi.org/10.1002/qj.222.

D. P. Donovan, H. Klein Baltink, J. S. Henzing, S. R. de Roode, and A. P. Siebesma. A depolarisation lidar-based method for the determination of liquid-cloud microphysical properties. *Atmospheric Measurement Techniques*, 8(1):237–266, 2015. doi: 10.5194/amt-8-237-2015. URL http://www.atmos-meas-tech.net/8/237/2015/.

G. Feingold, L.A. Remer, J. Ramaprasad, and Y.J. Kaufman. Analysis of smoke impact on clouds in brazilian biomass burning regions: an extension of twomeys' approach. *Journal of Geophysical research*, 2001.

Graham Feingold, Wynn L Eberhard, Dana E Veron, and Michael Previdi. First measurements of the Twomey indirect effect using ground-based remote sensors. doi: 10.1029/2002GL016633.

D. A. Hegg, D. S. Covert, H. H. Jonsson, and R. K. Woods. A simple relationship between cloud drop number concentration and precursor aerosol concentration for the regions of Earth's large marine stratocumulus decks. *Atmospheric Chemistry and Physics*, 12(3):1229–1238, 2012. ISSN 16807316. doi: 10.5194/acp-12-1229-2012.

Yoram J Kaufman, Ilan Koren, Lorraine A Remer, Daniel Rosenfeld, Yinon Rudich, and Veerabhadran Ramanathan. The effect of smoke, dust, and pollution aerosol on shallow cloud development over the Atlantic Ocean.

Byung-Gon Kim. Effective radius of cloud droplets by ground-based remote sensing: Relationship to aerosol. *Journal of Geophysical Research*, 108(D23):4740, 2003. ISSN 0148-0227. doi: 10.1029/2003JD003721. URL http://doi.wiley.com/10.1029/2003JD003721.

Byung-Gon Kim, Stephen E. Schwartz, Mark A. Miller, and Qilong Min. Effective radius of cloud droplets by ground-based remote sensing: Relationship to aerosol. *Journal of Geophysical Research: Atmospheres*, 108 (D23):n/a–n/a, 2003. ISSN 2156-2202. doi: 10.1029/2003JD003721. URL http://dx.doi.org/10.1029/2003JD003721. 4740.

James D. Klett. Anomalous diffraction model for inversion of multispectral extinction data including absorption effects. *Appl. Opt.*, 23(24):4499–4508, Dec 1984. doi: 10.1364/AO.23.004499. URL http://ao.osa.org/abstract.cfm?URI=ao-23-24-4499.

D. Koch and A. D. Del Genio. Black carbon semi-direct effects on cloud cover: Review and synthesis. *Atmospheric Chemistry and Physics*, 2010. ISSN 16807316. doi: 10.5194/acp-10-7685-2010.

LASIC. lasic. URL https://www.arm.gov/research/campaigns/amf2016lasic. Accessed: 2017-04-06.

A McComiskey and G Feingold. The scale problem in quantifying aerosol indirect effects. *Atmospheric Chemistry and Physics*, 12(2):1031–1049, 2012.

Qilong Min and Lee C Harrison. Cloud properties derived from surface MFRSR measurements and comparison with GOES results at the ARM SGP site. 23(13):1641–1644, 1996.

Detlef Müller, Albert Ansmann, Ina Mattis, M. Tesche, Ulla Wandinger, Dietrich Althausen, and G. Pisani. Aerosol-type-dependent lidar ratios observed with Raman lidar. *Journal of Geophysical Research Atmospheres*, 2007. ISSN 01480227. doi: 10.1029/2006JD008292.

ORACLES. oracles. URL https://espo.nasa.gov/missions/oracles/content/ORACLES_Science_Overview_0. Accessed: 2017-04-06.

S. R. Pal and A. I. Carswell. Polarization anisotropy in lidar multiple scattering from atmospheric clouds. *Appl. Opt.*, 24(21):3464–3471, Nov 1985. doi: 10.1364/AO.24.003464. URL http://ao.osa.org/abstract.cfm?URI=ao-24-21-3464.

M. Pinsky, A. Khain, I. Mazin, and A. Korolev. Analytical estimation of droplet concentration at cloud base. *Journal of Geophysical Research: Atmospheres*, 117(D18):n/a–n/a, 2012. ISSN 2156-2202. doi: 10.1029/2012JD017753. URL http://dx.doi.org/10.1029/2012JD017753. D18211.

C.M.R. Platt. Remote sounding of high clouds. iii: Monte carlo calculations of multiple-scattered lidar returns. *Journal of atmospheric sciences*, 1980.

Measures Raymond. Electromagnetic theory of radiation. In *Laser remote sensing, fundamentals and applications*, pages 11–58. Krieger publishing company, 1984. ISBN 0894646192.

M.L. Salby. Academic Press, 1995. ISBN 0-12-615160-1.

K. Sarna and H W J Russchenberg. Ground-based remote sensing scheme for monitoring aerosol-cloud interactions. *Atmospheric Measurement Techniques*, 2016. ISSN 18678548. doi: 10.5194/amt-9-1039-2016.

K. Sarna, M. de Graaf, and Herman W J Russchenberg. tropical cloud and smoke properties measured by a UV-lidar on Ascension Island. 2016.

A. F. Stein, R. R. Draxler, G. D. Rolph, B. J. B. Stunder, M. D. Cohen, and F. Ngan. Noaa's hysplit atmospheric transport and dispersion modeling system. *Bulletin of the American Meteorological Society*, 96(12):2059–2077, 2015. doi: 10.1175/BAMS-D-14-00110.1. URL http://dx.doi.org/10.1175/BAMS-D-14-00110.1.

Garstang M. Macko S.A. Tyson P.D. Maenhaut W. Artaxo P. Kalberg-P. Talbot R. Swap, R. The long-range transport of southern african aerosols to the tropical south atlantic. *journal of geophysical research*, 1996.

Matthias Tesch, Silke Gross, Albert Ansmann, Detlef Muller, Dietriech Althausen, Volker Freundenthaler, and Michael Esselborn. Profiling of saharan dust and biomass-burning smoke with multiwavelength polarization raman lidar at cape verde. *Tellus B*, 63(4):649–676, 2011. ISSN 1600-0889. doi: 10.1111/j.1600-0889.2011.00548.x. URL http://dx.doi.org/10.1111/j.1600-0889.2011.00548.x.

S. Twomey. the influence of pollution on th shortwave albedo of clouds. 1977a.

S. Twomey. Elsevier scientific publishing company, 1977b. ISBN 0-444-41527-0.

Ulla Wandinger, Holger Baars, Ronny Engelmann, Anja Hünerbein, Stefan Horn, Thomas Kanitz, David Donovan, Gerd-Jan Van Zadelhoff, David Daou, Jürgen Fischer, Jonas Von Bismarck, Florian Filipitsch, Nicole Docter, Michael Eisinger, Dulce Lajas, and Tobias Wehr. HETEAC: THE AEROSOL CLASSIFICATION MODEL FOR EARTHCARE. 2016. doi: 10.1051/epjconf/201611901004.

A

Appendix

A.1. Lidar parameters

Table A.1: Lidar calibration constants used during this study.

Constant	Value
Xt	0.02
Cr	1.0/0.026
Clid	9.5
dClid	1.0

A.2. Cloud properties

Table A.2: Overview of the selected cloud parts. The '# measurement' column shows the number of lidar measurements of this selection. A minimum of five is required for the cloud retrieval inversion algorithm. The start and end altitude column gives the boundaries of the height of the selection.

Date	start time [h]	end time [h]	# measurements	time span [minutes]	start altitude [m]	end altitude [m]
20160905	2.91	3.0	11	5.4	1000	1600
	4.14	4.2	7	3.5	1100	1700
	6.02	6.06	5	2.5	1000	1600
20160906	1.85	2.19	40	20.2	1000	1600
	4.5	5.3	96	48.0	1070	1670
	7.6	8.28	82	40.8	1240	1840
	8.78	9.3	62	31.2	1260	1860
	20.55	20.62	8	4.2	1180	1780
20160908	0.21	0.7	59	29.4	970	1567
	0.8	1.57	92	46.2	950	1550
20160909	6.1	6.5	48	24.0	700	1300
	12.8	13.3	60	30.0	1225	1825
	19.2	19.35	18	9.0	850	1450
20160910	0.7	0.9	24	12.0	970	1570
	4.28	4.8	62	31.2	990	1599
20160912	9.29	9.39	12	6.0	1000	1600
	9.6	10.22	74	37.2	980	1580
	18.86	18.94	10	4.8	870	1470
	20.9	21.22	38	19.2	730	1330
20160913	5.41	6.0	71	35.4	920	1520
	10.0	10.45	54	27.0	990	1590
	20.8	20.94	17	8.4	960	1560
	23.18	23.4	26	13.2	700	1300
20160915	9.1	9.31	25	12.6	860	1460
	10.85	11.3	54	27.0	930	1530
20160919	21.02	21.46	53	26.4	460	1060
	22.0	22.15	18	9.0	550	1150
20160920	19.25	19.4	18	9.0	580	1180
20160921	20.0	21.0	120	60.0	510	1110
	22.44	22.85	49	24.6	700	1300
20160922	1.3	1.9	72	36.0	700	1300
	2.9	4.0	132	66.0	700	1300
	4.5	5.4	108	54.0	700	1300
	5.6	6.2	72	36.0	700	1300
	8.53	9.6	128	64.2	700	1300
	10.0	11.0	120	60.0	760	1360
20160923	4.79	4.91	15	7.3	972	1191
	7.12	9.6	298	148.8	560	1160
	12.6	13.8	144	72.0	700	1300
	20.6	21.58	118	58.8	700	1300
	21.9	22.7	96	48.0	630	1230
20160924	3.6	4.48	106	52.8	800	1400
20160929	5.97	6.2	28	13.9	850	1450

Table A.3: Overview of the weighted mean and standard error of the mean of the cloud properties per selected cloud part obtained by the cloud property retrieval algorithm. The '# measurement' column shows the number of values obtained by the retrieval and used for the averaging.

Date	mean time [h]	# measurements	R_{eff} [μm]	$\sigma_{wR_{eff}}$ [μm]	α [m^{-1}]	$\sigma_{w\alpha}$ [m^{-1}]	ND [cm^{-3}]	σ_{wND} [cm^{-3}]	cbh [m]	σ_{cbh} [m]
20160905	2.96	2	3.37	0.29	0.03	0.0	573.29	80.82	1235.2	10.3
	4.17	1	3.57	0.93	0.07	0.01	1134.11	609.21	1281.0	0.0
	6.04	1	3.35	0.52	0.04	0.0	709.59	278.06	1302.2	0.0
20160906	2.03	7	3.3	0.12	0.03	0.0	449.57	44.97	1347.5	21.1
	4.9	16	3.19	0.14	0.03	0.0	393.84	46.75	1368.1	23.2
	7.95	14	3.57	0.15	0.04	0.0	501.46	59.83	1535.6	16.3
	9.03	10	3.34	0.12	0.03	0.0	425.93	60.84	1599.2	20.8
	20.58	1	3.91	1.6	0.06	0.01	886.08	864.77	1472.3	0.0
20160908	0.46	10	3.74	0.24	0.03	0.0	328.29	40.54	1271.9	11.3
20160909	6.3	8	3.13	0.05	0.03	0.0	567.05	44.52	1085.7	66.0
	13.05	10	3.42	0.18	0.03	0.0	284.61	45.9	1510.9	26.0
	19.28	3	3.03	0.33	0.05	0.0	1075.4	176.33	1153.5	10.9
20160910	0.8	4	4.37	0.05	0.02	0.0	264.67	12.07	1282.1	9.7
	4.53	10	3.77	0.31	0.03	0.0	258.75	40.13	1264.8	10.1
20160912	9.34	2	3.32	0.46	0.03	0.0	301.8	163.14	1307.8	6.5
	9.9	12	3.17	0.07	0.03	0.0	480.2	62.93	1281.0	8.4
	18.91	2	4.48	0.14	0.03	0.0	292.11	25.17	1181.0	6.5
	21.05	6	3.09	0.06	0.02	0.0	445.26	55.05	1103.1	32.5
20160913	5.71	12	3.31	0.09	0.03	0.0	484.11	40.92	1260.9	23.0
	10.23	9	3.35	0.11	0.04	0.0	561.16	54.87	1313.4	24.6
	20.87	3	3.1	0.22	0.05	0.0	977.9	125.48	1275.2	15.3
	23.28	4	4.0	0.2	0.02	0.0	227.89	22.28	1047.8	15.9
20160915	9.2	4	3.28	0.2	0.03	0.0	393.15	55.88	1151.5	15.0
	11.08	9	3.06	0.06	0.03	0.0	518.88	43.56	1191.9	46.1
20160919	21.24	9	1.88	0.18	0.03	0.0	1196.56	134.17	761.9	16.2
	22.08	3	2.78	0.07	0.03	0.0	928.12	48.48	841.2	8.5
20160920	19.32	3	1.93	0.3	0.04	0.01	1690.07	307.88	882.3	9.7
20160921	20.5	20	2.64	0.02	0.02	0.0	693.53	25.37	837.5	35.2
	22.64	8	2.91	0.05	0.03	0.0	670.46	51.34	996.8	16.9
20160922	1.6	12	2.83	0.06	0.03	0.0	693.34	36.8	1014.2	42.4
	3.45	22	3.01	0.03	0.03	0.0	596.77	30.74	1025.9	28.5
	4.95	18	2.96	0.02	0.03	0.0	729.67	20.87	995.1	21.2
	5.9	12	2.84	0.04	0.03	0.0	807.95	26.69	992.1	22.6
	9.06	21	2.96	0.03	0.03	0.0	662.77	22.83	1032.0	21.0
	10.5	20	2.94	0.04	0.03	0.0	802.81	20.2	1041.1	16.6
20160923	8.37	50	2.72	0.02	0.02	0.0	604.74	18.74	892.1	57.7
	13.2	24	2.84	0.06	0.03	0.0	564.12	41.06	952.0	42.8
	21.1	20	2.8	0.04	0.03	0.0	806.08	25.1	986.4	31.1
	22.3	16	3.04	0.04	0.03	0.0	671.2	30.35	984.3	74.3
20160924	4.05	18	3.38	0.05	0.05	0.0	728.24	35.03	1111.7	10.0
20160929	6.09	5	3.21	0.05	0.04	0.0	736.93	24.97	1131.1	18.8

A.3. Aerosols - clear sky

Table A.4: Overview of the selected clear sky parts. The '# measurement' column shows the number of lidar measurements of this selection.

Date	start time [h]	end time [h]	# measurements	time span [minutes]
20160905	15.7	16.2	60	30.0
	16.5	17.2	84	42.0
20160906	3.2	4.2	120	60.0
	6.6	7.4	96	48.0
	18.15	18.32	20	10.2
	22.19	22.26	8	4.2
20160907	19.5	20.1	72	36.0
20160908	1.85	1.98	16	8.05
	20.55	20.65	12	6.15
20160909	2.54	2.63	11	5.55
	20.19	20.3	13	6.6
	23.09	23.2	13	6.6
20160910	2.05	2.39	41	20.35
	5.2	5.8	72	35.99
	19.0	19.29	35	17.4
	20.45	20.9	54	27.0
20160912	19.89	20.1	25	12.72
	21.83	21.95	14	7.03
20160913	21.45	21.51	7	3.6
20160915	20.27	20.43	19	9.4
	21.75	21.85	12	5.96
20160919	6.9	7.3	48	24.0
20160920	6.7	7.09	47	23.4
	16.6	17.46	103	51.36
	21.2	21.77	68	34.2
	22.3	22.9	72	36.0
20160921	0.0	0.29	35	17.3
	21.31	21.44	16	7.8
20160923	4.46	4.7	29	14.4

A.4. Aerosol-cloud Interactions

Table A.5: The results of the IE calculations. The date, mean time and number of measurements with the resulting IE values with uncertainty are presented for each cloud selection. The '# measurement' column shows the number of values obtained by the retrieval. Only selected parts with more than 2 measurements were included.

Date	mean time [h]	# measurements	IE_r	IE_N
20160906	2.03	7	0.42±0.16	-1.063±0.51
	4.9	16	-0.359±0.02	0.955±0.04
	7.95	14	-0.558±0.12	3.193±0.6
	9.03	10	-1.022±0.81	2.096±2.13
20160908	0.46	10	0.247±0.09	-0.753±0.75
20160909	6.3	8	0.008±0.01	0.099±0.05
	13.05	10	-0.529±0.27	1.47±0.92
	19.28	3	-0.992±-0.03	1.264±-0.01
20160910	0.8	4	0.061±inf	-0.278±inf
	4.53	10	-0.443±0.3	0.867±0.46
20160912	9.9	12	-0.409±0.17	0.631±0.52
	21.05	6	-0.204±0.04	0.227±0.13
20160913	5.71	12	-0.306±0.07	0.734±0.25
	10.23	9	0.057±0.01	-0.17±0.05
	23.28	4	-0.08±inf	-0.006±inf
20160915	9.2	4	-0.146±inf	-0.164±inf
	11.08	9	0.012±0.01	-0.107±0.02
20160919	21.24	9	-0.389±0.06	0.54±0.09
	22.08	3	0.457±-0.0	0.969±-0.01
20160920	19.32	3	-1.268±-0.09	1.275±-0.48
20160921	20.5	20	-0.12±0.01	-0.003±0.02
	22.64	8	-0.138±0.14	-0.142±0.47
20160922	1.6	12	-0.076±0.01	0.094±0.02
	3.45	22	0.01±0.01	-0.09±0.03
	5.9	12	0.195±0.0	-0.161±0.02
	9.06	21	0.116±0.01	0.196±0.02
	10.5	20	0.791±0.08	-0.157±0.07
20160923	13.2	24	-0.004±0.01	0.058±0.04
	21.1	20	-0.218±0.01	0.43±0.02
	22.3	16	-0.021±0.0	0.047±0.01
20160924	4.05	18	0.497±0.06	-1.404±0.14
20160929	6.09	5	0.069±0.04	-0.129±0.09